Journal of Electronic Materials (2022) 51:6082–6107
https://doi.org/10.1007/s11664-022-09846-7

REVIEW ARTICLE

Absorption Coefficient of Bulk III-V Semiconductor Materials: A Review on Methods, Properties and Future Prospects

Hui Jing Lee[1] · Mansur Mohammed Ali Gamel[2] · Pin Jern Ker[3] · Md Zaini Jamaludin[1] · Yew Hoong Wong[4] · John P. R. David[5]

Received: 15 June 2022 / Accepted: 21 July 2022 / Published online: 23 August 2022

Abstract

Over the last few decades, research works have focused on elucidating the optical properties of semiconductor materials. Despite remarkable progress in the measurement and calculation of the absorption coefficient for semiconductor materials, there is a lack of comprehensive review on the comparative study of absorption coefficient properties for different types of bulk semiconductor materials and their methods for calculating the absorption coefficient. Hence, this paper summarizes the fundamentals of the various methods used to determine the absorption coefficient properties of bulk growth semiconductor crystals, and discusses their advantages and disadvantages. Furthermore, this review provides comprehensive results from recent studies and findings on the absorption properties of near- to mid-infrared (wavelengths from 800 to 7300 nm) group III-V semiconductor materials. In addition, the absorption coefficient of the conventional group IV semiconductors (silicon and Ge) were included for performance comparison. Critical analysis was done for the reviewed materials concerning their material properties, such as band gap structure, crystal quality, and the structural design of the device. The related studies on the methods to determine the absorption coefficients of semiconductors and to improve the likelihood of absorption performance were well highlighted. This review also provides an in-depth discussion on the knowledge of absorption coefficient based on a wide range of semiconductor materials and their potential for sensors, photodetectors, solar and photovoltaic application in the near to mid infrared region. Lastly, the future prospects for research on absorption coefficients are discussed and the advancement in the determination of absorption coefficients for new ternary and quaternary materials is proposed using artificial intelligence such as neural networks and genetic algorithm.

Keywords Semiconductor material · absorption coefficient · ternary · quaternary

Introduction

Research on optical properties such as the absorption coefficient (α) of semiconductor materials in various structures has gained significant interest owing to their importance in optoelectronics, photonics and quantum technologies. Specifically, α represents the penetration depth of photons into the material before it is absorbed for any particular wavelength.[1] Precise selection of material influences the performance of devices significantly. This is because α predicts the minimum detectivity of a material and plays a crucial role in designing high-performance lasers, sensors,[2] imaging devices, information processing, communication devices, and energy harvesters.[3–5] For example, understanding the absorption properties of semiconductor material is essential to design the best combination of hybrid structures for photovoltaic (PV) applications.[6]

✉ Hui Jing Lee
LHJing@uniten.edu.my

1 Department of Electrical & Electronics Engineering, Institute of Power Engineering, Universiti Tenaga Nasional, 43000 Kajang, Malaysia

2 Electronic Engineering Department, Universitat Politècnica de Catalunya, Jordi Girona 1-3, 08034 Barcelona, Spain

3 Department of Electrical & Electronics Engineering, Institute of Sustainable Energy, Universiti Tenaga Nasional, 43000 Kajang, Malaysia

4 Department of Mechanical Engineering, Faculty of Engineering, Universiti Malaya, 50603 Kuala Lumpur, Malaysia

5 Department of Electronic and Electrical Engineering, The University of Sheffield, Firth Court, Western Bank, Sheffield S10 2TN, UK

In this regard, α is worth studying both numerically and experimentally. To attain the optical absorption coefficient of various semiconductor materials and their structures, there are several well-known and mature methods to solve for α, including transmission (Swanepoel envelope method), the combination of transmission and reflectance, spectral ellipsometry (SE), transfer matrix, photocurrent measurement derivation and interpolation.[7–9] Different methods for calculating and measuring α yield results with varying accuracy and consistency. The semiconductor properties and structural designs affect the optical absorption properties. Therefore, it is crucial to understand α of different materials, which is dependent on the device structure. A detailed characterization of α as a function of wavelength helps to predict the optical behavior properties and to design semiconductor devices with high optical performance.

Over the last few decades, research on α has received tremendous attention due to the importance of matching the α value of semiconductor materials in a vast range of applications, and there is a good amount of research work on this subject. However, the research work is limited to the comparison of methods for determining α of silicon (Si),[10] the effect of various temperatures on α[11] and solving the α of new semiconductor material.[12] Currently, there is no reported work which provides critical review and discussion on the experimental measurement and calculation of α. Therefore, this review aims to provide an in-depth analysis of the absorption coefficient properties of different semiconductor materials together with the possible enhancement of the computation of α. The structure of the paper is as follows. "Fundamentals of Absorption Coefficient in Direct- and Indirect-Bandgap Material" section introduces the operating principles of absorption coefficient. "Absorption Coefficient Measurement and Calculation Method" section presents the various methods to obtain the absorption coefficient for single layer and multiple layers structures. In addition, their respective advantages and disadvantages with regard to recent improvement will be discussed. "Absorption Coefficient in Different Types of Semiconductor Materials" section summarizes the absorption coefficient findings for different types of group III-V and group IV materials such as Si, germanium (Ge), indium arsenide (InAs), indium antimonide (InSb), gallium arsenide (GaAs), gallium antimonide (GaSb), indium phosphide (InP), indium gallium arsenide (InGaAs), indium gallium antimonide (InGaSb), indium arsenide antimonide (InAsSb), indium gallium phosphide (InGaP), gallium arsenide bismuth (GaAsBi), gallium arsenide nitride (GaAsN), indium gallium arsenide phosphide (InGaAsP), indium gallium arsenide antimonide (InGaAsSb), indium gallium arsenide nitride (InGaAsN) and gallium arsenide bismuth nitride (GaAsBiN). These materials have cutoff wavelengths in the near- to mid-infrared region (800–7300 nm), which can be utilized in crucial applications such as gas sensing, imaging and photovoltaics. This review provides clear and accessible guidance on the different methods for calculating and measuring the absorption coefficient and their suitability for use with various semiconductor materials.

Fundamentals of Absorption Coefficient in Direct- and Indirect-Bandgap Material

There are two types of interband absorption mechanisms, namely direct- and indirect-bandgap absorption. The valence and conduction bands occur in the same momentum for the direct-bandgap material, while the momentum is different for the indirect-bandgap material.[13] Generally, direct-bandgap material absorbs light better than indirect-bandgap material, especially near the cutoff wavelength. In such case, direct-bandgap material would be a better option for a thin active layer.[14] Also, the temperature variation has a more significant effect on the absorption spectrum of indirect-bandgap material as compared to direct-bandgap material.

In general, α represents the loss of wave amplitude information and is expressed as an exponential decay function which can be derived from the propagation of Poynting vector $\langle S_z \rangle$ in a homogeneous medium with respect to refractive index (n) and extinction coefficient (k). S_z is expressed as the real part of the cross product of electric field (E) and complex conjugate magnetic field (H) as shown below[15]:

$$\langle S_z \rangle = \frac{1}{2}\mathrm{Re}\left[E_x \times H_y^*\right] \tag{1}$$

$$\langle S_z \rangle = \frac{1}{2}\mathrm{Re}\left[E_o \exp\left(\frac{i\boldsymbol{n}}{c}z\right) * \frac{E_o^* N^*}{\mu_o c}\exp\left(\frac{-i\omega \boldsymbol{n}^*}{c}z\right)\right] \tag{2}$$

where E_o is the amplitude of the electric field, ω is the angular frequency, $\boldsymbol{n}$ is the complex refractive index $= n + ik$, μ_o is the vacuum permeability, and c is the speed of light in vacuum. Upon the simplification of Eq. 2, $\langle S_z \rangle$ is equal to

$$\langle S_z \rangle = \frac{1}{2}\frac{|E_o|^2}{\mu_o c} n \exp\left(\frac{-4\pi k}{\lambda}z\right) \tag{3}$$

In this regard, it is crucial to identify the α of semiconductor materials while understanding the wave penetration through the medium.

Absorption Coefficient Measurement and Calculation Method

There are several methods to calculate and perform predictive analysis on the absorption coefficient of semiconductor materials. Optical measurement methods such as transmission, reflection and SE measurements can be

used to determine the α. Furthermore, the combination of transmission and reflection measurements, Swanepoel's envelope method and transfer matrix can improve the accuracy of the α data. Measurement such as photocurrent can be used to calculate the α using the external quantum efficiency (EQE) or responsivity curves information. On the other hand, interpolation is used to estimate the α of new compound materials using the absorption data of their original materials. This method is useful for ternary and quaternary materials. Hence, this section briefly discusses on the characteristics of different methods, and performs a critical discussion on the suitability of methods for various types of materials.

Transmission and Reflection Measurements for Structure with a Single Absorber Layer

Transmission (T) measurement is an accurate method to determine the optical behavior below the fundamental absorption edge.[16] The conventional way of measuring the transmittance through a homogeneous medium is by taking the ratio of transmitted light intensity, I_T to the intensity of incoming light, I_o. The absorption coefficient of material is calculated using the Lambert–Beer law[16]:

$$I_T = I_o e^{-\alpha(\lambda)d} \tag{4}$$

where d is the thickness of the material. In this case, the reflection at the material interface is made negligible. Nevertheless, transmission measurement requires a transparent substrate where sample preparation such as substrate etching is crucial prior to the measurement process. It is worth highlighting that transmission measurement is not suitable for translucent material because the diffusion and scattering of an incident beam would influence the result accuracy. Also, despite having high accuracy at the band edge when semiconductor layers are grown on a transparent substrate, the accuracy is reported to be less consistent when the transmission reading approaches zero.[17,18]

Moving on, Swanepoel's envelope method is a simple, fast and accurate approach to determine the α of material and was introduced in 1983.[19] It is capable of calculating $\alpha(\lambda)$ using the transmission spectrum that displays clear interference fringes.[20] This method is used to determine the α of the film thickness, together with the complex refractive index for the material. However, Swanepoel's envelope method might fail if the absorption in the film is so high that interference fringes are not visible where maximum envelope and minimum envelope curves coincide. Furthermore, the method becomes less accurate with decreasing film thicknesses in the micrometer range. This occurs when the absorption band falls in the range of the interference extreme. In principle, Swanepoel's envelope is found to be a simple, reliable and accurate method to calculate the absorption of samples with uniform thickness.[21] For example, Swanepoel's envelope method is used to evaluate the spectral dispersion and α for amorphous selenium and cadmium telluride (CdTe) thin films, and the results show consistency for samples with uniform thicknesses.[22,23] Moreover, the transmission method has limitations in measuring ultrathin film material and material with a high absorption value. Therefore, research efforts should focus on the two highlighted limitations. Jin et al.[9] demonstrated an improvement in the Swanepoel method by incorporating a tangent point method (TPM), which is able to calculate the thickness and optical behavior of the material. This improvement yielded a 0.5% improvement in accuracy in calculating α of chalcogenide material with an abnormal thickness value in the strong absorption region.

Recently, Swanepoel's envelope method can be found in numerous commercial software.[24,25] Several fitting equations for transmission analysis are widely used in commercial software such as Filmwizard and TfCalc for optical design analysis of α for thin film materials. The commonly used models are the Cauchy equations, Sellmeier relation, Forouhi–Bloomer dispersion relations, Lorentz classical oscillator model and Drude model.[18] Recently, Jena et al.[26] introduced a user-friendly software program, PRISA, which is able to retrieve transmission spectra using n and k data. In addition, the thickness of the material is calculated using Swanepoel's envelope method. The graphical interface of PRISA is less tedious than other software, while producing an accurate result.

Furthermore, reflection measurements (R) are also commonly used to determine n, k and α unknowns of thin film materials[16,27] using spectroscopy measurement. The R spectrum can be measured either using the calibrated mirror in reference position or V-W setup, which are common calibration methods used for reflectance standards.[28] There are two types of reflection, namely the specular reflection and diffusion reflection or the combination of both. It is essential for the samples to have optically polished surfaces to ensure constant power reflectance over the surface. With R measurement, the absorption coefficient in the single-layer structure is expressed using Eq. 5.[29,30]

$$\frac{I_T}{I_0} = \frac{\left[(1-R)^2 + 4R\sin^2\theta\right]\exp(-\alpha l)}{1 - R^2\exp(-2\alpha l)} \tag{5}$$

where I_T is the transmitted current, I_0 is the incidence current, l is the device thickness, $\theta = \tan^{-1}\left[\frac{2k}{n^2+k^2-1}\right]$. For simplification purposes in calculating the absorption parameter, θ is made negligible in the measurements.[30]

The combination of T and R measurements improves the accuracy of the α data. For example, it is recommended that the T measurement coupled with the estimated R of

the materials be used to determine α.[31] Huang et al.[32] presented an accurate model using the T and R measurements to determine α, considering the internal reflection of light within the thin film. The combined T and R method is a simple and direct way to obtain the $\alpha(\lambda)$ data. However, in a scenario where the film is not perfectly homogeneous, it is nearly impossible to measure $T(\lambda)$ and $R(\lambda)$ at the exact spot on the film,[16,27] which leads to inconsistency and lower precision in the results.[18] Additionally, the thickness of the indirect-bandgap semiconductor material is crucial to study the indirect resonant absorption. In 2018, the $\alpha(\lambda)$ of Ge with different thicknesses was determined using T and R methods. It is reported that Ge with thicknesses $d = 0.175$ mm and 1.04 mm are too thin to generate accurate results close to the absorption edge, notably that the result only converges for thickness > 2 mm. Moreover, the theoretical and experimental α results in the intermediate energy show a good agreement. Therefore, thickness of sample becomes a significant influencing parameter for an accurate α measurement near the absorption edge using the T and R methods.[33] T and R measurements are preferred for material with near-IR absorption because surface reflection shows minimum variation at the near-IR region and is most often negligible. However, it is more challenging to interpret α for material with mid-IR spectra, because the reflection of the front surface material can interrupt the result analysis on the penetration that occurs through the material.[32]

Transmission and Reflection Measurements for Multilayer Structure Using the Transfer Matrix Method

The transfer matrix method (TMM) analyzes the absorption coefficient for propagation that occurs through layered materials.[34] It takes the interference effect into account through a coherent wave superposition as opposed to intensity superposition.[35] There are two types of transfer matrixes, namely the transmission matrix and propagation matrix. A transmission matrix is used to calculate the fields across an interface, while a propagation matrix is applicable for estimating the propagation across distance in any homogeneous medium.[36,37] Commonly, TMM is a powerful mathematical tool used to perform light propagation analysis for multilayer dielectric media.[8] Physical properties of the material and boundary conditions are taken into careful account for TMM to accurately solve for the α behavior. It is widely used to calculate α for acoustic metamaterial for an oblique incidence,[38,39] perovskite solar cells (PSCs),[40] multilayer perforated panel systems,[41] and multilayer graphene.[34] TMM is then further modified for multilayer acoustic materials,[42] material with coherent, partially coherent and incoherent interference.[43] In 2015, Deng et al.[44] modified the TMM with electromagnetic boundary conditions required by Maxwell's equation taking into account both transverse electric and magnetic waves. The breakthrough improvement has enabled the TMM to determine the α of any layer in all position of the media.

One major advantage of TMM is that there is no constraint in terms of the thickness of the layer which makes TMM a suitable modeling structure for multilayer material. TMM also has the advantage of handling structure with difference in index between the composite materials. Moreover, the drawback of TMM is that it is only suitable for continuous wave propagation; Fourier transform needs to be incorporated to solve for pulse propagation which increases the complexity of the mathematical computation.[45] Another limitation of TMM is that the simulation procedure assumes that the plane orthogonal to the direction of propagation expands in infinite manner where such a scenario is unrealistic in a real case. To accommodate this, the material layers have to be broad enough to avoid the assumption error in wave propagation.[45] For multilayer structure, the TMM calculation is done for each layer using matrix relation. The mathematical computation time is relatively long as there is lack of mathematical model and tool to relate the change in the field between the layers. Hence, TMM appears to be useful for calculating the α of a multilayer structure and the analysis of surface waves which involve a different planar interface. Nevertheless, the properties and boundary condition of each material layer must be carefully defined whereby the complexity of the matrix solver and derivatives appear to be a challenge which often requires longer computation time.

In 2018, by incorporating TMM, photoluminescence (PL) is used to identify the $\alpha(\lambda)$ of multilayer thin films, taking into account the absorption effect of the front layer and substrate.[8] It is worth noting that PL is extremely sensitive and is, for example, able to solve for very low $\alpha \sim 10^{-16}$ cm^{-1} for Si material,[46] the α below the bandgap is obtained with generalized Planck's law based on the luminesce emission due to indirect transition in Si. Moreover, PL is reported to have scientific limitations where multiple excited states may exist in the optical centers.

Spectroscopic Ellipsometry

SE was proposed by Drude[47] and was later experimentally demonstrated by Ingersoll and Littleton[48]. It is a non-destructive method that extracts both n and k using the polarization of incident light reflected from the measured samples.[49,50] In conventional ellipsometry measurement, the setup consists of a light source, sample, and receiver. The light source consists of monochromatic light and polarization generator, while the detector consists of a polarization analyzer and detector. SE is a method used to calculate α for a broadband light source condition, where the effect of

change in light polarization is taken into account.[51,52] Owing to its measurement sensitivity, SE is suitable for broadband light source material, thin films, transparent material, semi-opaque layers and substrates.[53,54] For example, SE is used to study the optical absorption spectrum for graphite and graphene flakes on transparent substrate.[55] Most importantly, SE has also appeared to be reliable in measuring the absorption coefficient of semiconductor at phonon energy higher than the band edge region.[56]

The SE method measures the distance of absorption occurrence instead of measuring the reflective intensities, it reports the actual absorption information across the thicknesses of the material which is more accurate compared to the transmission method and is preferred to solve for α of new materials. For example, recent findings from Chandan et al.[12] preliminarily conducted a study of absorption properties of a new material, PPDT2FBT polymer, for optoelectronic devices using SE. In 2020, Samarasingha et al.[57] also implemented SE to model the optical properties of ZnO layers on Si and SiO_2 for wide-bandgap (0.03–6.5 eV) applications. Moreover, SE is a promising method for modeling the optical properties of new semiconductor materials compared to other methods owing to its sensitivity and accuracy. SE can provide information on the thickness, refractive index and dielectric function of residual oxides and intentionally formed sulfides, as investigated by Papis et al.[58]

SE is a powerful, reliable, repeatable and highly useful method for analyzing thin film and substrates, with high precision in optical characterization reported. However, the method has limitations in accounting for extreme surface sensitivity in which very thin contamination on the samples lead to inconsistency in the result.[18] Moreover, SE has the ability to determine the properties of unknown material in the case where it is a single layer grown on a known substrate material. In addition, a sample of surface material must be smooth and flat for SE. Measurement for multilayer structure appears to be less useful using SE because the material properties of each intermediate layer must be measured in a separate manner for a better precision of results.

Photocurrent Method

Moreover, α can also be calculated from the experimental photocurrent measurement by applying the current continuity equation. In such circumstances, it is assumed that all carriers generated in the depletion region contribute to the photocurrent.[59,60] Based on the photocurrent measurement, α of semiconductor materials can be determined with the responsivity and EQE calculations.

Responsivity Calculation

Responsivity calculation is preferred for semiconductor devices where absorption has fully taken place in the intrinsic region.[61] The responsivity, R, is measured using the photocurrent method and evolved to be the main parameter used to calculate the absorption coefficient.[61,62]

$$\alpha = -\frac{1}{W_1}\ln\left(1 - \frac{R}{1-R_p}\frac{hv}{q}\right) \tag{6}$$

in which the W_1 is the thickness of the i-region of the semiconductor, hv is the incident photon energy, q is the elementary electric charge, and R_p is the reflection coefficient of the material. As illustrated in Fig. 1, Eq. 6 can be used to calculate the absorption coefficient of the i-region material, the main absorber region. Meanwhile, the bandgap of the p-region material is larger than that of the absorber region material, which makes it transparent to the absorption spectrum of interest. In a direct-bandgap semiconductor, where the incident photons have energy higher than the bandgap, α is described using the Tauc relation[61,63]:

$$\alpha(hv) \propto (hv - E_g)^{\frac{1}{2}} \tag{7}$$

where E_g is the bandgap of the material.

It is worth mentioning that this solution is suitable for semiconductor material with a short cutoff wavelength, where absorption is likely to occur at the first layer of material. In contrast, if this calculation is used for materials with an infrared cutoff wavelength, α data would have high error. This phenomenon is very likely to occur, as the equation does not take into account other electrical and optical performance parameters of the structure. In this case, α is solely proportional to the responsivity of the material. Furthermore, the success of this solution requires the use of fully fabricated devices with suitable metallic contacts.

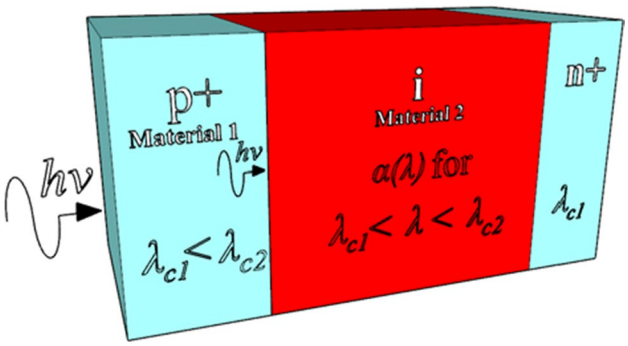

Fig. 1 PIN junction with transparent P layer.

EQE Calculation

The absorption coefficient of the material can be solved iteratively with the EQE information together with the detail of the specific material and cell structure, which are carefully identified. EQE calculation appears to be more complex, as it is conducted with the photocurrent measurement taking into account detailed information of the cell regions and material composition. For example, in a device with p^+-i-n^+ which correlates with the α of material[5,64] as illustrates in Fig. 2, EQE(λ) is expressed as:

$$\mathrm{EQE}(\lambda) = (1 - R)(\eta_\mathrm{P} + \eta_\mathrm{i} + \eta_\mathrm{n}) \tag{8}$$

where R is the reflectivity as a function of wavelength, λ, which is related to n and k:

$$R(\lambda) = \frac{[n(\lambda) - 1]^2 + k^2(\lambda)}{[n(\lambda) + 1]^2 + k^2(\lambda)} \tag{9}$$

Meanwhile, η_P, η_i and η_n represent the EQE of the p^+, i and n^+ regions, respectively, contributed by several design parameters expressed as follows:

$$\eta_\mathrm{p} = \left[\frac{\alpha L_\mathrm{e}}{\alpha^2 L_\mathrm{e}^2 - 1}\right]\left[\frac{\frac{S_\mathrm{e}L_\mathrm{e}}{D_\mathrm{e}} + \alpha L_\mathrm{e} - \exp\left(-\alpha X_1\right)\left(\frac{S_\mathrm{e}L_\mathrm{e}}{D_\mathrm{e}}\cosh\left(\frac{X_1}{L_\mathrm{e}}\right) + \sinh\left(\frac{X_1}{L_\mathrm{e}}\right)\right)}{\frac{S_\mathrm{e}L_\mathrm{e}}{D_\mathrm{e}}\sinh\left(\frac{X_1}{L_\mathrm{e}}\right) + \cosh\left(\frac{X_1}{L_\mathrm{e}}\right)} - \alpha L_\mathrm{e}\exp\left(-\alpha X_1\right)\right] \tag{10}$$

$$\eta_\mathrm{i} = (\exp[-\alpha X_1])(1 - \exp[-\alpha(X_2 - X_1)]) \tag{11}$$

$$\eta_\mathrm{n} = \left[\frac{\alpha L_\mathrm{h}}{\alpha^2 L_\mathrm{h}^2 - 1}\right][\exp[-\alpha(X_3 - X_2)]]\left[\alpha L_\mathrm{h} - \frac{\frac{S_\mathrm{h}L_\mathrm{h}}{D_\mathrm{h}}\left[\cosh\left(\frac{X_3}{L_\mathrm{h}}\right) - \exp(-\alpha X_3)\right] + \sinh\left(\frac{X_3}{L_\mathrm{h}}\right) + \alpha L_\mathrm{h}\exp(-\alpha X_3)}{\frac{S_\mathrm{h}L_\mathrm{h}}{D_\mathrm{h}}\sinh\left(\frac{X_3}{L_\mathrm{h}}\right) + \cosh\left(\frac{X_3}{L_\mathrm{h}}\right)}\right] \tag{12}$$

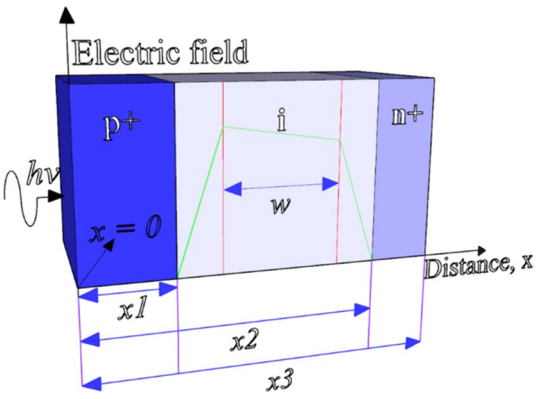

Fig. 2 Electric field profile of a PIN junction. The red line is the electric field profile of an ideal PIN whereas the blue line is a non-ideal PIN, assuming the intrinsic region is n-doped (Color figure online).

where L_e (L_h) is the diffusion length of electrons (holes), D_e (D_h) is the diffusion coefficient of electrons (holes), S_e (S_h) is the surface recombination of electrons (holes), X_1 is the distance from the top surface to the depletion edge in the p^+ region, X_2 is the distance from the top surface to the depletion edge in the n^+ region, and X_3 is the total thickness of the p^+-i-n^+ layers as demonstrated in Fig. 2. The diffusion length is expressed using the relationship between the diffusivity and lifetime of the minority carrier. $L_\mathrm{e} = \sqrt{D_\mathrm{e}\tau_\mathrm{e}}$, where L_e represents the diffusion length, and τ_e is the lifetime of a minority carrier.

For the case where penetration happens in the short wavelength region, the surface recombination of electrons is high, and Eq. 10 is simplified as

$$\eta_\mathrm{p} = \left[\frac{\alpha L_\mathrm{e}}{\alpha^2 L_\mathrm{e}^2 - 1}\right]\left[\frac{1}{\sinh\frac{X_1}{L_\mathrm{e}}} - \alpha L_\mathrm{e}\exp\left(-\alpha X_1\right)\right] \tag{13}$$

The capacitance–voltage (C–V) measurement is used to determine the depletion width, w. The p^+-i-n^+ layers are labeled as shown in Fig. 2, in which the thickness of the p^+ and p^+ structures can be obtained from secondary ion mass spectroscopy (SIMS) measurement. The doping concentrations affect parameters such as L_e (L_h), D_e (D_h) and τ_e (τ_h).

Subsequently, L_e and L_h can be determined by measuring the responsivity under illumination. Otherwise, they can be calculated using the mathematical model equations for D_e (D_h) and τ_e (τ_h). Upon identifying the parameters and the EQE from the responsivity measurement, α can be solved numerically.

EQE calculation yields high α accuracy, as the mathematical model considers the diffusion length, surface recombination and diffusion coefficient of electrons and holes. The other advantage of the method is that it can determine the ultralow α value of semiconductors, which cannot be identified using the transmission and reflectance methods.[6] Furthermore, it is suitable for semiconductors with short cutoff wavelengths where a majority of the absorption occurs in the p region, and a simplification of the equations

is possible. Published research work has determined the α of the material, with the assumption that the α happen only in the p-region.[59,60] On the other hand, if the illuminated photons pass through all the p-i-n regions, the computation of α would be much more challenging. This is because there are six unknown variables (L_e, L_h, D_e, D_h, S_e and S_h) to be estimated in Eqs. 8–12, and α is very sensitive to their variations. Moreover, the accuracy of EQE calculation depends on the device fabrication with appropriate metal contacts which appears to be a limitation for the photocurrent method.

In addition, extracting the photocurrent information from measurement also appears to be challenging as photocurrent spectrum requires a suitable benchmarking device accounting for the photocurrent generation in the desired spectrum. Other important factors that could potentially contribute to the measurement error should be elucidated. For example, the incoming beam is required to have a bigger spot size on the device area with an even coverage, and the intensity of a light beam coming from the focusing lens should fall evenly on the device to ensure the photocurrent landing on the device is accurately measured. These procedures are necessary to minimize the possibility that yield measurement uncertainties or result error.

Interpolation Method

Interpolation is commonly used to estimate the α of new ternary and quaternary compound materials based on α of their binary compounds. Using the Thompson-Woolley Empirical Fit formula as a function of the material composition,[65] α for ternary and quaternary materials can be approximated. In those cases, the accuracy of α for new semiconductor materials would rely heavily on the accuracy of α for the binary compounds. For instance, the accuracy of α for InGaAs would be dependent on the α data of binary compounds InAs and GaAs, while the accuracy of α for InGaSb would be dependent on the α data of binary compounds InSb and GaSb. α estimation was demonstrated for $In_{0.53}Ga_{0.47}As$[66,67] and $In_{0.19}Ga_{0.81}Sb$[68] as a function of x composition with respect of the tertiary material, $A_xB_{1-x}C$

$$\alpha(E) = x\alpha_1(E - E_g + E_1) + (1 - x)\alpha_2(E - E_g + E_2) \quad (14)$$

x = material composition; E_g = material bandgap; E_1 = bandgap semiconductor AC; E_2 = bandgap semiconductor BC; α_1 = absorption of AC; α_2 = absorption of BC.

On the other hand, the α of quaternary semiconductor materials, for example, InGaAsSb and InAsSbP, can be determined using the $A_xB_{1-x}C_yD_{1-y}$ relationship[69]:

$$\alpha(E) = xy\alpha_1(E - E_g + E_1) + x(1 - y)\alpha_2(E - E_g + E_2) + (1 - x)y\alpha_3(E - E_g + E_3) + (1 - x)(1 - y)\alpha_4(E - E_g + E_4) \quad (15)$$

x = material composition; y = material composition; E_g = material bandgap; E_1 = bandgap semiconductor AC; E_2 = bandgap semiconductor AD; E_3 = bandgap semiconductor BC; E_4 = bandgap semiconductor BD; α_1 = absorption of AC; α_2 = absorption of AD; α_3 = absorption of BC; α_4 = absorption of BD.

Interpolation appears to be advantageous to mathematically derive and approximate the α of ternary and quaternary semiconductor materials such as InGaAs,[70] InGaSb,[68,71] InGaP,[72] InGaAsP[73] and InGaAsSb.[74,75] Such an approach would provide prediction of the α based on the alloy property and composition. The α of mature material such as $In_{0.53}Ga_{0.47}As$ was studied both numerically and experimentally. For example, Burkhard et al.,[76] Humreys et al.[77] and Bacher et al.[78] experimentally validated the α of $In_{0.53}Ga_{0.47}As$ using SE, transmission and reflectance. Nevertheless, the accuracy of the interpolated α data for new composition of quaternary materials such as lattice-mismatched InGaAs are yet to be further confirmed with experimental work.[79]

The main downside of interpolation is that the derivation appears to be impossible for new semiconductor materials where the input data are not readily available. Recently, a study investigated the improvement of the interpolation method where the accuracy of the method is further improved using a morphing algorithm which maps the critical points of the absorption material of materials based on their material composition.[80] This approach is useful in the case where the complex refractive index of material is unknown; moreover, other parameters such as refractive indices and bandgap energy of the initial material composition need to be clearly identified to accurately model the optical property of the material.

Table I summarizes the advantages, disadvantages, and fundamental characteristics of α measurement and calculation methods for different types of semiconductor materials. In general, transmission and reflectance methods are the most popular for obtaining the α of single-layer semiconductor materials due to their simplicity. Transmission and reflectance spectra can be used to determine the α in very simple steps. Nevertheless, it is nearly impossible to measure transmittance and reflectance at the same spot on the film,[16,27] which reduces the effectiveness of this method. Also, transmission has the limitation of low accuracy with ~ 20% of error. Swanepoel's envelope method, on the other hand, can solve for both thickness and α of the film with a 1% relative error in the absorption coefficient range of about 100 cm^{-1} to 5×10^4 cm^{-1}.[19] The transfer matrix method is beneficial

Table I Summary of measurement and calculation methods for calculating the α of semiconductor material.

Method	Advantages	Disadvantages	Thickness	Accuracy	Recommendations
Transmittance	Simple setup and calculation method	Not accurate for $\alpha > 10^3$ cm^{-1} as the transmission approaches zero and the detection of the output is less sensitive[17] Reflection between the boundaries of each material complicates the calculation. Therefore it must be grown on a transparent substrate[81]	Suitable for film samples with thicknesses of a few microns.	An approximated error of 20 %[17] Required a smooth surface for accrued measurements	Preferred at the absorption band edge up to 10^3 cm^{-1}.
Swanepoel's envelope	Suitable for any appreciable transmission spectrum and interference fringes [82] It can be used to obtain the thickness of sample	The method might fail if the absorption in the film is so high that interference fringes are not visible and $TM(\lambda)$ and $Tm(\lambda)$ curves coincide	Suitable for thick samples, and it cannot handle local absorption features if the film is not very thick [18]	An approximated error of 1% [19] Accuracy decreases with the decrease of film thickness	For material with abnormal thickness value in the strong absorption region
Transmission and reflectance	Simple and direct method [27, 32] Non-destructive methods	Nearly impossible to measure transmittance and reflectance at exactly the same spot on the film [16, 27] It is very difficult to obtain sufficiently accurate absolute specular reflectance data [18]		It depends on the accuracy of the measured transmissivity and refractive index [32]	–
Transfer matrix	Calculate α within the interfaces of the structure with infinite cell layer absorption	The calculation is much more complicated	No restriction and suitable for multilayer material that is stacked together [45]	–	For multilayer structure with careful information on boundary condition
Spectroscopic ellipsometry	Extreme surface sensitivity [18] Non-destructive method	Long time to identify the polarization of each wavelength and requires a simulator via a computer [47] Not suitable for higher absorption coefficients (greater than 10^4 cm^{-1})	Suitable for thin films and substrates [54]	More accurate than transmission method since it shows the distance where the absorption occurs instead of measuring the absolute reflective intensity Accuracy depends on the surface roughness and the exciting of native oxide [18]	For broadband light source material
Photocurrent	Detailed derivation for semiconductors after considering the absorption of photons and collection of carriers	Calculation tends to be a complicated derivation if the absorption is expanded in multiple layers The α can only be selected for a range of wavelengths to eliminate the absorption impact which may happen on layers other than absorber Requires a device with metal contacts	–	Relies on the photocurrent measurement and the conduction the accurate assumptions	Estimates the optical absorption in the semiconductor device after considering the generation and resistance losses

Table I (continued)

Method	Advantages	Disadvantages	Thickness	Accuracy	Recommendations
Interpolation	Theoretical and fast estimation before the measurement Suitable for new quandary and binary materials Does not require measurement	Estimating method Difficulty to trace error as it combined more than two measurements	–	The accuracy of the baseline materials will significantly affect the estimation	For new binary, ternary and quaternary materials

for multilayer material, as this method considers the optical effect of all the device layers. In addition, the SE method is accurate, with promising sensitivity. However, it is difficult to measure a high absorption value with this method ($> 10^4$ cm^{-1}). The last two methods in Table I are the electrical- and interpolation-based methods. Firstly, photocurrent measurement uses the EQE and responsivity curves to calculate α. This method gives a comparatively accurate result, provided that all the parameters of the material structure are precisely identified. Lastly, interpolation has the ability to use data of the reported α of binary materials to estimate α for ternary and quaternary material with a variation in element composition. Table II lists and maps the types of semiconductor materials with their suitable type of measurement or calculation method, which will be further discussed in "Absorption Coefficient in Different Types of Semiconductor Materials" section..

Absorption Coefficient in Different Types of Semiconductor Materials

Light absorption of semiconductor materials is the most crucial parameter to consider when designing PV cells and photodetectors. It varies based on the optical properties, bandgap and crystal structure of the materials. Therefore, it is crucial to understand the optical performance of different materials and room for improvement in terms of optical behavior with their respective structural design and potential applications. This section reviews the findings of optical properties and their respective applications for several III-V compound semiconductor materials such as InAs, InSb, GaAs, GaSb, InP, InGaAs, InGaSb, InAsSb, InGaP, GaAsBi, GaAsN, InGaAsSb, InGaAsP, InGaAsN and GaAsBiN. To provide a comparative study on the optical absorption property, this section starts with a brief review of the conventional group IV elements such as Si and Ge. For each type of material, the absorption coefficient spectrum and mechanism are highlighted alongside the measurement methods. The significance of the absorption coefficient improvement and their potential application for the materials are discussed and proposed accordingly.

Single-Element Semiconductor Material

Si (1.14 eV) and Ge (0.67 eV) are promising single-element materials for many semiconductor applications. While Si has the advantage of cost-effectiveness,[133] Ge possesses a narrower bandgap, which allows it to operate in the infrared region.[134] Both materials have an indirect bandgap, which means that the transition of an electron from the maximum energy level in the valance band to the minimum energy level in the conduction band involves not only photons

Table II Summary of semiconductor materials with suitable types of measurement/calculation methods.

Method	Material														
	Si	Ge	GaAs	GaSb	InAs	InSb	InP	InGaAs	InAsSb	InGaSb	InGaP	GaAsN	GaAsBi	InGaAsP	InGaAsSb	GaInAsN
Transmittance	83, 84	33, 85	86–88	89	90, 91		92–95	31, 96	97–99	100	72	101, 102				103
Swanepoel's envelope	83															
Transmission and reflectance	83	104, 105		106	107	108		77, 78								
Transfer matrix			109					110								
Spectroscopic ellipsometry	111, 90, 1, 112	93, 113	93, 114	90, 92, 115	92	63, 116, 117	76	76	118		119			120	121, 122	
Photocurrent					123–126					127			102, 128, 129		130	131
Interpolation								132	97	68	119			66	74, 75	

with energy equal to or more than the bandgap energy but also phonons, which corresponds to atomic vibration. The vibration helps to generate the needed momentum to transfer electrons to the conduction band. In this case, α is low for photons with energies near the band edge and increases rapidly when the photon energy is higher than the indirect bandgap.[135]

The $\alpha(\lambda)$ is the sum of photon and phonon absorption expressed as[136]:

$$\alpha(\lambda) = \alpha_a(\lambda) + \alpha_e(\lambda) \tag{16}$$

The $\alpha_a(\lambda)$ can be represented as:

$$\alpha_a(\lambda) = \frac{A\left(E - E_g + E_p\right)^2}{\exp\left(\frac{E_p}{kT}\right) - 1} \tag{17}$$

where E is the photon energy, E_p is the energy of the absorbed photon, T is the temperature in Kelvin and k is Boltzmann's constant.

The $\alpha_e(\lambda)$ is represented as:

$$\alpha_e(\lambda) = \frac{A\left(E - E_g - E_p\right)^2}{1 - \exp\left(\frac{-E_p}{kT}\right)} \tag{18}$$

With regard to Si, the direct bandgap is about 3.4 eV, and the indirect bandgap is near 1.1 eV. Therefore, it is vital to study the optical properties of Si for wavelength ranges between 300 and 1100 nm. At the indirect-bandgap region, α has a contribution from the emission or absorption of phonons.[84] Figure 3a shows $\alpha(\lambda)$ of Si using different methods. Overall, the graph portrays those various methods generate identical α values for Si. It is important to note that film temperature affects the absorption as expressed in Eqs. 17 and 18, and α of Si under the variation of temperature was measured by Bucher et al.[83] In a detailed study, three different methods were used to calculate the discrepancies of experimental results in the UV and IR spectra. To illustrate, transmission (T), SE and normal-incidence reflection measurement methods were used when $\alpha(\lambda) < 10^4$ cm^{-1}, between 10^3 cm^{-1} and 10^6 cm^{-1} and $> 5 \times 10^5$ cm^{-1}, respectively.[83] However, $\alpha(\lambda)$ had a similar trend to SE, T and transmission and reflectance (T&R) methods when λ ranged from 200 to 1050 nm.[10,90,93,112] In 2013, Wang et al.[84] investigated the α of 10 µm ultrathin single-crystal Si using the T method, with an uncertainty value of 5–7%. It was found that the measured data was comparable to the best available data and models. Meanwhile, α of intrinsic silicon is calculated using Kramers–Kronig relation,[111] where the α and optical parameters of Si were studied under a temperature of 300 K and in the range of 250–1450 nm. The $\alpha(\lambda)$ at a wavelength of 250 nm is 1.84×10^6 cm^{-1}, while $\alpha(\lambda)$ at 1450 nm is 3.2×10^{-8} cm^{-1}.

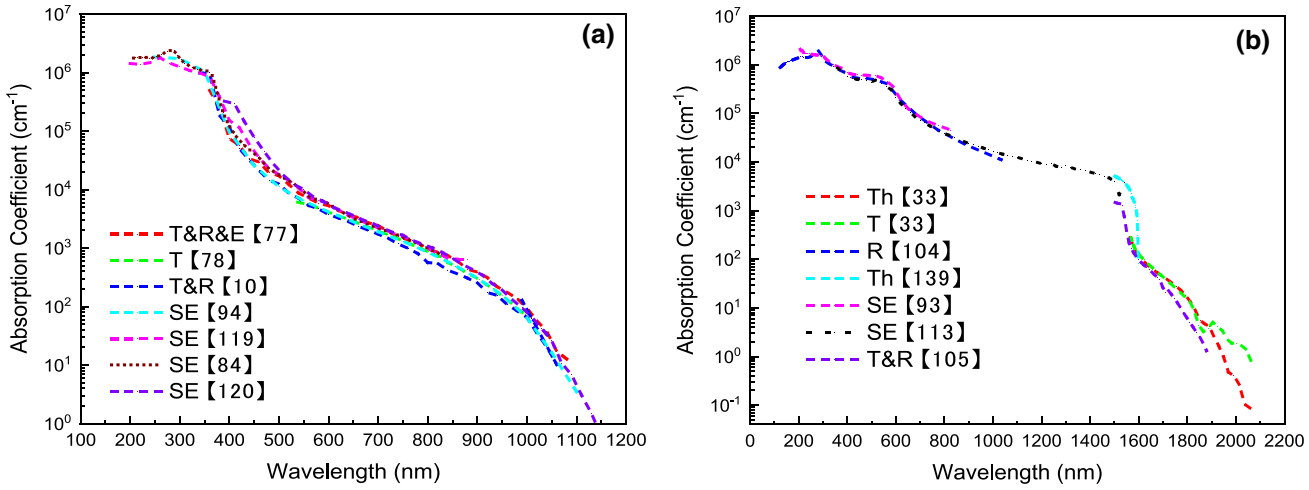

Fig. 3 Methods to calculate the α for (a) Si film, (b) Ge film; Th is theoretical calculation.

On the other hand, $\alpha(\lambda)$ of Ge varies from λ of 200 to around 1800 nm, and the measurement of optical properties range from 0.6 eV to 11.3 eV was conducted back in 1959 using the Kramers–Kronig relation, in which the absorption peak is recorded at 4.4 eV.[104] In 1973, α of Ge with a thickness of 10.6 µm was studied.[137] The theoretical challenge regarding Ge was highlighted as its indirect-bandgap energy is only ~ 0.1 eV, which is lower than the lowest direct optical transition. Figure 3b shows $\alpha(\lambda)$ of Ge using various methods. Menendez et al. [33] had taken into account the excitonic effect with intermediate states. This assumption affects α of Ge with an additional resonant enhancement. Based on Fig. 3b, the absorption coefficient data reported by various works are agreeable. It is worth mentioning that different methods are of preference for the different ranges of wavelengths. For example, the R method was mainly used for shorter λ,[104] whereas the SE method was reported by Aspnes et al.[93] and Tsao et al.[113] for short λ up to 1600 nm. T and T&R methods are preferred for $\lambda > 1600$ nm.[33,105] Additionally, Liu et al.[138] studied the Cody-Lorentz model and characterized the optical absorption of Ge thin film on Si substrate using electron beam evaporation. It was found that the absorption and reflection of the Ge film are greater than the bulk material since the decay rate of the former in the longwave direction is lower than that of the latter due to the presence of a tail state in the Ge film material. A recent study by Huang et al.[139] shows that Ge grown on Si has better absorption at 1550 nm, as illustrated in Fig. 3b.

To conclude, it is observed that α of Ge drops dramatically at $\lambda > 1550$ nm while the α reduction trend starts to occur at $\lambda > 400$ nm for Si. This happens solely because the direct bandgaps of Ge and Si are 0.9 eV and 3.4 eV, respectively. Hence, the likelihood of photon absorption with energy lower than the material's direct bandgap is significantly low. Furthermore, the α values of Si and Ge are well established, and future studies should focus on improving its characteristic for various applications. To illustrate, in 2018, Guo et al.[140] presented an enhancement in $\alpha(\lambda)$ for a Si cell near the band edge using Fourier series-based periodic nanostructures. In addition, one of the main applications for the Ge semiconductor material is in TPV cells, as it has a bandgap of 0.66 eV which gives a wide spectral response that matches the majority of the TPV heat sources. However, it has the disadvantage of high reverse current and low open-circuit voltage, which outweighs the benefits. In a recent study, Gamel et al.[141] demonstrated the use of a Ge absorber layer with thickness of 150 µm. The design was able to produce output performance equivalent to that a an InGaAs TPV cell, but at the expense of a very thick absorber layer. In this regard, future research should extend the study on improving the absorption performance of Ge TPV cells using an optimum absorber layer.

Binary Semiconductor Material

GaAs (1.42 eV), GaSb (0.726 eV), InAs (0.354 eV), InSb (0.17 eV), and InP (1.34 eV) are direct III-V semiconductor materials receiving increased attention in LED and laser applications due to their behavior in luminescent and optoelectronics devices.[142] GaAs and GaSb operate in the visible region and the beginning of mid-infrared radiation, showing great potential for laser diodes, photodetectors, tandem solar cells and TPV applications.[143,144] Meanwhile, InAs and InSb are found to be sensitive in the far-IR region, which makes them suitable for applications in infrared systems and detectors, thermal imaging cameras, high-speed electronics, forward-looking infrared radar (FLIR) systems, and TPV for radiation temperatures < 1000 K.[145,146] For direct-bandgap materials, the transition of an electron from the maximum energy level in the valance band to the minimum energy

level in the conduction band involves only photons with energy equal to or greater than the bandgap energy. In addition, the probability of absorption depends on the density of electrons equipping the internal energy and density of an empty state at final energy. Both values increase with energy away from the band edge. The $\alpha(\lambda)$ can be represented as follows[147]:

$$\alpha(\lambda) = A_{\text{direct}} * \sqrt{\frac{1.24}{\lambda} - \frac{1.24}{\lambda_c}} \tag{19}$$

where A_{direct} in $\text{cm}^{-1}\ \text{eV}^{-1/2}$ is a constant value that varies with different direct semiconductor materials, λ is the photon wavelength, and λ_c is the cutoff wavelength of the material. Usually, α is only measured for limited photon energy. Equation 19 can also be used to do a curve fitting and to estimate the absorption in the absence of complete experimental data. For example, the A_{direct} of GaSb, InGaAs, InGaAsP and InGaAsSb is 22,600 $\text{cm}^{-1}\ \text{eV}^{-1/2}$, 22,900 $\text{cm}^{-1}\ \text{eV}^{-1/2}$, 36,600 $\text{cm}^{-1}\ \text{eV}^{-1/2}$ and 26,000 $\text{cm}^{-1}\ \text{eV}^{-1/2}$, respectively.[148,149]

Focusing on GaAs material, Strurge et al.[114] studied α for thicknesses from 6 mm to 0.6 µm, with photon energy between 0.6 eV and 2.75 eV, and a temperature range of 10–294 K. The α is low for photon energy 0.6–1.4 eV mainly because of the ionization of impurities. At 1.5 eV, absorption due to the formation of excitons is observed which can be explained using Elliot's theory. On the other hand, a constant α value of $1.4 \times 10^5\ \text{cm}^{-1}$ was reported for photon energy higher than 1.5 eV up to 2.75 eV. In 1987, Goni et al.[109] investigated the direct and indirect absorption for GaAs. The reported result showed that the strength of direct absorption increases linearly with the energy level of direct gap and the direct absorption edge is at a thickness between 2 µm and 4 µm. In comparison, indirect absorption occurs at a thickness of 30 µm. In 1961, Moss et al.[150] derived the absorption of GaAs in the range of 1 cm^{-1} to $10^4\ \text{cm}^{-1}$ based on T measurement on single-crystal GaAs, and the absorption edge was observed at 4000 cm^{-1}. Different methods are used to determine the α of GaAs, and as illustrated in Fig. 4a, they obtain approximately similar results. For example, the reported α using the T method,[88,151] the SE method[152] and other methods[72,92,153] show consistent trends with minimum discrepancy. Based on the published work, the impurity concentration affects α at wavelengths near the cutoff wavelength of the semiconductor material. For example, at 77 K cell temperature, as the n-doped GaAs varied from $3 \times 10^{17}\ \text{cm}^{-3}$ to $9.6 \times 10^{17}\ \text{cm}^{-3}$, $\alpha(\lambda)$ at 840 nm (corresponding to bandgap energy of 1.475 eV) was reported to vary from 20 cm^{-1} to 10 cm^{-1}.[86] In addition, Casey et al.[87] presented the concentration dependence of α for *n*- and *p*-type GaAs for a bandgap between 1.3 eV and 1.6 eV with T measurement in the range $10 \le \alpha \le 10^3\ \text{cm}^{-1}$. Meanwhile, *p*-type GaAs records α of 225 cm^{-1}, where free-carrier absorption (FCA) is about 3 cm^{-1}. For Zn-doped p+ material at a heavy concentration of $7 \times 10^{19}\ \text{cm}^{-3}$, α was 250 cm^{-1}. This is chiefly due to the FCA.

Turning to GaSb, Munoz et al.,[115] Ferrini et al.,[154] Adachi,[92] Abroug[89] and Aspnes et al.[93] experimentally measured α of GaSb using the SE method, as shown in Fig. 4b. The study discussed that the high α of GaSb in the infrared region makes it a suitable candidate for PV and TPV applications. Furthermore, Chandola et al.,[106] Qiao et al.[155] and Akiniami et al.[156] presented α of GaSb using the T&R method for multiple layers, while the T method[89,156] reported slightly lower α than other reported methods.[90,93,155] Furthermore, Wang et al.[157] used the model dielectric function method to evaluate the thermal radiation-dependent performance of a GaSb TPV cell. By referring to the model dielectric function, α of GaSb is found to be manipulated by the critical points in the electronic band structure. The calculated α is in agreement with the experimentally collected data using the SE method.

For the InAs material, α of *n*-type InAs in the fundamental absorption edge region is studied for a temperature range from 18 K to 300 K in 1961 using the T method.[91] The origin where α starts to roll off for InAs is similar to that of InSb and GaSb at the long wavelength near the absorption edge. Figure 4c shows the absorption coefficient curves of InAs material measured via various methods. Similarly, the T method is used to obtain α for visible radiation up to the extended infrared region.[90,151,158] Moreover, α was studied using the R method,[93] while Dixon et al.[91] investigated it for a carrier concentration range from 3.6×10^{16} to $3.8 \times 10^{18}\ \text{cm}^{-3}$, and they found that lower carrier concentration contributes to a higher α. In addition, the SE method[92] reported a similar trend to the R method[91] and the T method[90] at low doping concentration. In other work, α of InAs was measured in the range of 2500 cm^{-1} to 260 cm^{-1}. Recently, the enhancement of the below gap transmission of InAs single crystal using suppression of native defects was reported by Shen et al.[159] which is vital to improve the nonlinear bandgap absorption coefficient of InAs.

For InSb, Hiroshi and Robert[160] measured the reflectivity and transmissivity for InSb in the range of 20–200 µm. It was found that weak α is recorded at λ of 28.3 µm due to the overtone of lattice vibration. Additionally, α obtained via the T&R method[161] was slightly higher than the other reported data using the SE method,[93,108,116,117] as illustrated in Fig. 4d. The α values for wavelengths of 1.5–7.5 µm were measured by Moss et al.[108] using the T measurement. It was reported that for $\lambda < 4$ µm, α is proportional to $\frac{1}{\lambda}$. Furthermore, the α variation of n-doped InSb due to the

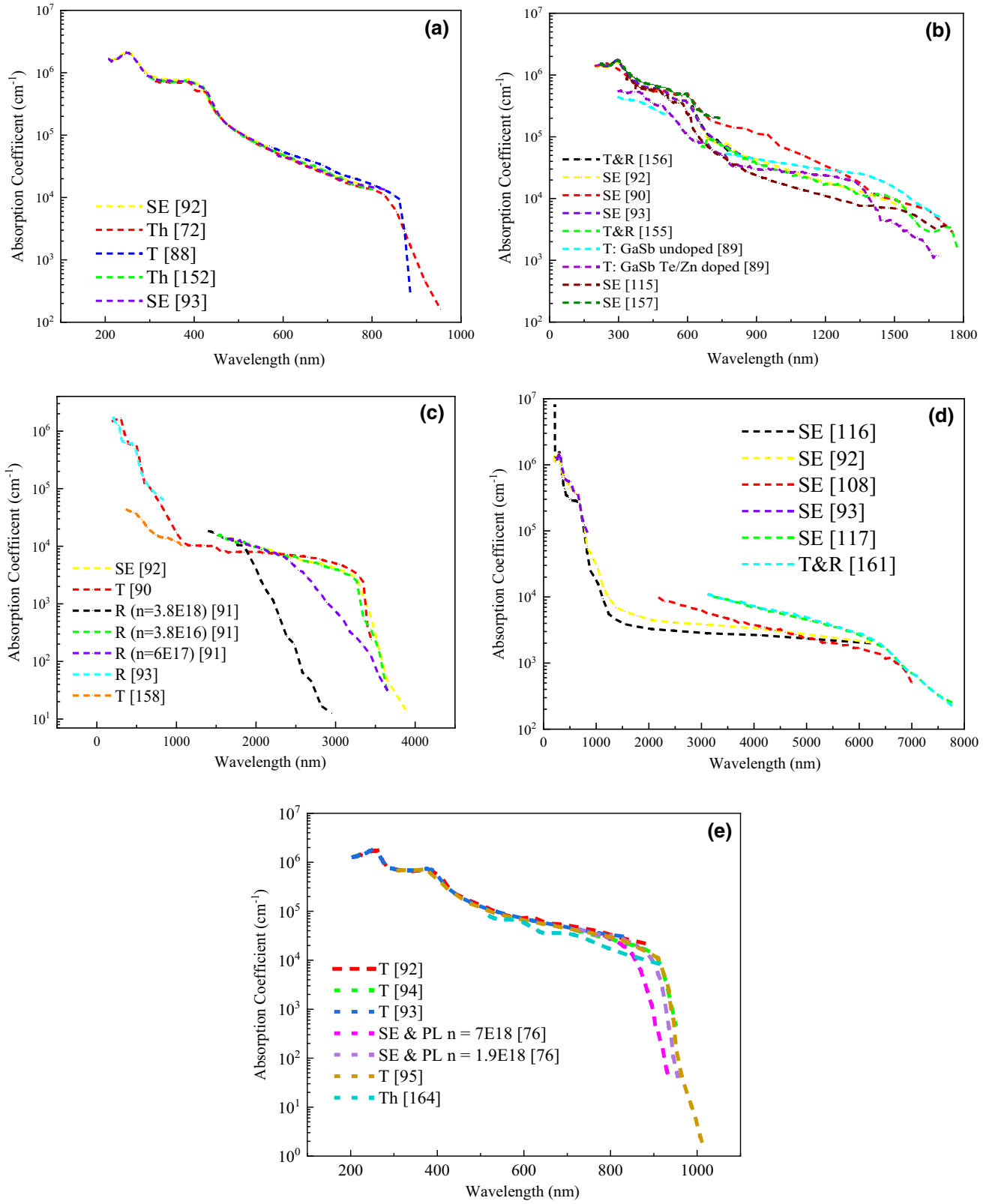

Fig. 4 Methods to calculate the α for (a) GaAs, (b) GaSb, (c) InAs, (d) InSb, and (e) InP.

change in doping concentration was investigated at 77 K and 130 K.[162] The impact of dopant on the interband and free-carrier absorption were studied. It is highlighted that a high dopant concentration of 10^{19} cm^{-3} or more is needed for the n-region to allow the diffusion of majority carriers to pass through the junction. Moreover, a high dopant concentration will cause high reflection and lead to a reduction in the photogeneration of charges.

InP with a bandgap of 1.34 eV (950 nm) has received tremendous attention in optical communications in the wavelength range of 900–1700 nm.[94] The direct-bandgap properties make it a valuable candidate for optoelectronic devices such as laser diode applications. It has high optical quality, which is commonly used as a lattice-matched substrate for InGaAs and InGaP photodetector material. In addition, engineering the absorption coefficient characteristics of low-cost InP thin-film photovoltaic devices is crucial in achieving optimum solar energy harvesting performance.[163] The research of Adachi et al.,[92] Aspnes et al.,[93] Dutta et al.,[94] Deng et al.[95] and Garcia et al.[164] reported a similar trend in absorption coefficient for InP as presented in Fig. 4e. It is well discussed that the direct transition occurs at 918 nm (1.35 eV) and 855 m (1.45 eV), while the indirect bandgap occurs at 561 nm (2.21 eV) and 604 nm (2.05 eV), respectively.[92] The absorption coefficient of InP at different doping concentrations was calculated by Burkhard et al.[76] using ellipsometry and photoluminescence effect. It is recorded that as the donor concentration increases, the absorption edge is flattened while the energy gap is slightly shifted to higher energy. This phenomenon is in agreement with the Burstein-Moss effect.

To conclude, binary materials are direct-bandgap semiconductors with various absorption spectra, making them suitable for various applications. Generally, α experiences a drastic drop when the energy of the photons is lower than the material bandgap because the likelihood of carrier transition is less effective. Furthermore, the increase in doping concentration reduces α and the cutoff wavelength as illustrated in Fig. 4c. The decreasing trend can be explained by the Moss-Burstein effect, which originates from the lifting of Fermi level above the conduction band due to the increase in charge carrier concentration.[165] To illustrate, at high doping concentration, all the states near the conduction band are populated. Therefore, electrons transitioning from the valance band need to shift to states above these populated states. The shift of the absorption edge to high energy levels is known as the Moss-Burstein shift.[166] With regard to the improvements, a recent study by Sai et al.[167] presented the enhancement of absorption performance for a thin-film GaAs solar cell using flattened light-scattering substrates. Furthermore, Qing et al.[168] demonstrated an enhanced light absorption by using a film-coupled metamaterial structure made from nanometer-thick GaSb sandwiched between a top layer of metallic grating and bottom layer of metal film. Furthermore, Wan et al.[169] discussed the design and optimization of the photonics crystal (PhC) structure to enhance optical absorption for GaAs and InAs absorption layers used in thin-film solar cells. Finally, InSb has more extended absorption spectra, making it applicable for antenna-coupled infrared detectors, photoelectric and magnet-electric conversion devices and optoelectronic devices. Despite the tremendous worldwide applications, the optical properties of this material are yet to be further studied in detail.[170]

Ternary Semiconductor Material

Semiconductor ternary compounds are composed of two binary compounds with adjustable bandgap energy, making it adaptable for various types of semiconductor applications.[171] For example, the bandgap energy of $In_{1-x}Ga_xAs$ can be engineered between 1.42 eV (GaAs) and 0.36 eV (InAs), which depends on the indium and gallium content ratio. Next, $InAs_{1-x}Sb_x$ is a narrow bandgap semiconductor with a bandgap (cutoff wavelength) of 0.1–0.413 eV (3000–12,000 nm).[98] $In_{1-x}Ga_xSb$ (0.248–0.73 eV bandgap, cutoff wavelength 1700–5000 nm) is another ternary material that belongs to the group III-V antimonides. It has several promising potential applications in TPV, sensors and photodetectors.[172–175] $In_{1-x}Ga_xP$ is a wide bandgap ~ 2 eV III-V material which is usually used as an absorber material for high-efficiency multijunction (MJ) solar cell application.[176] Lastly, the interesting changes in α for $GaAs_{1-x}N_x$ and $GaAs_{1-x}Bi_x$ with variation of nitrogen and bismuth composition are studied and compared.

The α and electrical properties of InGaAs were measured and simulated by Borrego et al.[132] in 1995. Interpolation was used to determine the α of $In_{0.50}Ga_{0.50}As$ via the weighted average of α from InAs and GaAs. Later in 1999, Wojtczuk et al.[31] calculated the α of $In_{0.72}Ga_{0.28}As$ (0.55 eV) using the T method, and numerical integration of α was performed to calculate the radiative combination coefficient. Jain et al.[70] determined the α of lattice-matched $In_{0.53}Ga_{0.47}As$ (0.74 eV) and lattice-mismatched $In_xGa_{1-x}As$ (0.6 eV) using interpolation modeling for a TPV application. As discussed earlier in "Interpolation Method" section, Burkhard et al.[76], Humreys et al.[77] and Bacher et al.[78] have experimentally validated the α of $In_{0.53}Ga_{0.47}As$ using SE, transmission and reflectance methods, which showed good agreement with the numerical results. For lattice-mismatched InGaAs, as highlighted in Fig. 5a, Alam et al.[177] mathematically derived the α of lattice-mismatched $In_{0.80}Ga_{0.20}As$, $In_{0.60}Ga_{0.40}As$, and $In_{0.20}Ga_{0.80}As$. The modeling tool was validated using the experimental work of lattice-matched InGaAs. This work provided a good reference and α validation tool for future experimental work in lattice-mismatched InGaAs. To date, there is limited study on α for extended InGaAs at a long

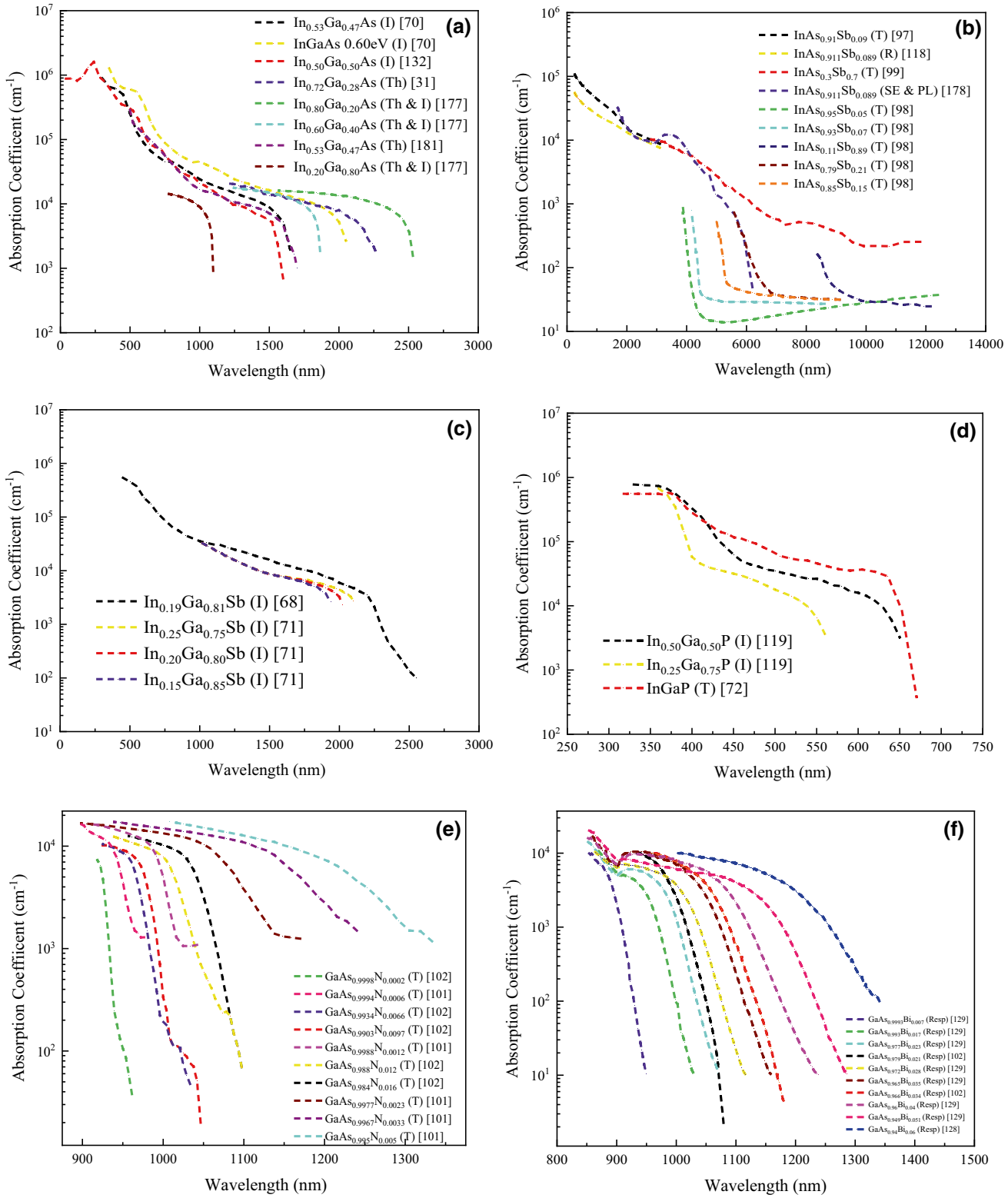

Fig. 5 Methods to solve α for (a) InGaAs, (b) InAsSb, (c) InGaSb, (d) InGaP, (e) GaAsN, and (f) GaAsBi; I represents interpolation.

cutoff wavelength. Therefore, it is significant to investigate the α of extended InGaAs to understand its potential functionality in IR semiconductor application such as waste heat harvesting.[141]

Turning to InAsSb, Stringfellow et al.[98] measured the α of $InAs_{0.95}Sb_{0.05}$, $InAs_{0.93}Sb_{0.07}$, $InAs_{0.11}Sb_{0.89}$, $InAs_{0.79}Sb_{0.21}$, and $InAs_{0.85}Sb_{0.15}$ using the T method shown in Fig. 5b. This pioneering research has provided an overview of a range of α for InAsSb with varying bandgap, in which the research focuses on solving the roll-off trends and cutoff wavelengths of the materials. There is room for improvement in terms of the accuracy of the results determined with the T method. Dobbelaere et al.[99] then calculated the α of $InAs_{0.30}Sb_{0.70}$ grown on GaAs using the T method. The α exhibited a roll-off at longer wavelength due to the higher Sb composition. The experimental result is consistent with the theoretical calculation. Recently, Zhang et al.[97] mathematically derived the α of $InAs_{0.91}Sb_{0.09}$ (0.286 eV) with $\lambda = 4330$ nm, yielding a value in close agreement with that of $InAs_{0.91}Sb_{0.09}$ measured by Marciniak et al.[118] using the R method, which shows the validity of InAsSb for TPV harvesting applications for the mid-IR region. In 2015, Webster et al.[178] measured the α of $InAs_{0.911}Sb_{0.089}$ using SE and PL methods. Two absorption peaks were recorded at 0.225 eV and 0.277 eV, respectively. This review reported a wide-ranging value of α in InAsSb at different bandgaps, so more research work is needed to study the properties of InAsSb for high-performance IR optoelectronics applications.

With regard to InGaSb, Refaat et al.[71] highlighted the functionality of InGaSb operating at 2000 nm for optical communication and atmospheric remote sensing application. The α of $In_{0.15}Ga_{0.85}Sb$, $In_{0.20}Ga_{0.80}Sb$, and $In_{0.25}Ga_{0.85}Sb$ was calculated using the interpolation method, as presented in Fig. 5c. In the reported result, α is higher at a shorter λ. The responsivity, however, decreases because of the severe effect of surface recombination. Zierack et al.[68] discussed the complexity of solving α for $In_{0.19}Ga_{0.81}Sb$ (0.5 eV), which demonstrates a roll-off in α after 2200 nm. The α was calculated by interpolating the α experimental result of InSb and GaSb. The results are significant to understand the performance of InGaSb cells for TPV application, which harvests IR. Prior to this, Plis et al.[100] measured the α of 2 µm-thick $In_{0.47}Ga_{0.53}Sb$ lattice-matched to $In_{0.36}Al_{0.53}Sb$ using the T method. To date, results reported on α for InGaSb are scarce; thus, α in the long wavelength region could be further studied and investigated.

Next, as mentioned earlier, InGaP is of particular interest for high-efficiency MJ solar cell applications.[176] For the case where multiple PV cells are connected in series, a wide-bandgap cell (> 2.0 eV) is needed to achieve the most efficient conversion of high-energy photons. Sun et al.[119] calculated the α of $In_{0.5}Ga_{0.5}P$ and $In_{0.25}Ga_{0.75}P$ (2.19 eV) as shown in Fig. 5d. Because of the limited data availability, α for $In_{0.25}Ga_{0.75}P$ was interpolated based on α of $In_{0.5}Ga_{0.5}P$ and InP. Recent work from Zhu et al.[72] reported the α of InGaP (1.89 eV) using the R method to design the most promising MJ device of an InGaP/GaAs/InGaAs structure. Notably, the reduced epitaxial layer thickness without compromising the α properties will lead to great cost reduction of the growth process of MJ.

GaAsN has been extensively studied for semiconductor lasers for optical-fiber communication in the wavelength range. GaAsN has a wide optical region coverage from the near infrared to the ultraviolet region, where the optical properties can be tailored as GaN and GaAs semiconductors. It is also highlighted that the smaller nitrogen will cause a big bandgap reduction, which causes GaAsN to have lower a bandgap value as compared to GaAs. For instance, 1% of nitrogen incorporation can contribute to a 0.2 eV bandgap reduction.[179] In 2000, Uesugi et al.[101] studied the absorption coefficient of $GaAs_{0.9966}N_{0.0034}$ and $GaAs_{0.992}N_{0.008}$ using the T method at 25 K and 297 K. The α^2 information was used to solve for the bandgap energy. It is observed that with higher nitrogen composition, the bandgap energies are lower. Later on, the absorption of $GaAs_{0.995}N_{0.005}$, $GaAs_{0.9967}N_{0.0033}$, $GaAs_{0.9977}N_{0.0023}$, $GaAs_{0.9988}N_{0.0012}$, $GaAs_{0.9994}N_{0.0006}$ and $GaAs_{0.9998}N_{0.0002}$ were measured using the T method.[180] The direct bandgap was calculated based on α and confirmed that GaAsN is a direct-bandgap material. The T method was also used to measure α of $GaAs_{0.984}N_{0.016}$, $GaAs_{0.988}N_{0.012}$, $GaAs_{0.9903}N_{0.0097}$, $GaAs_{0.9934}N_{0.0066}$, and $GaAs_{0.996}N_{0.004}$. As shown in Fig. 5e, it is observed that as the nitrogen composition increases with respect to GaAs, the absorption value decreases slowly before 8000 cm^{-1}.[102]

Lastly, GaAsBi has a low bandgap due to the bismuth composition and is a good candidate for MJ solar cells and low-noise semiconductor photodiodes. The effects on the photonics characteristics, specifically the valence band engineering, and α with the change in bismuth composition appear to be important features for further study. In 2012, Hunter et al.[128] studied α for $GaAs_{0.994}Bi_{0.006}$ using photocurrent measurement and confirmed that GaAsBi is a direct-bandgap material. It was reported that α demonstrates an exponential decrease with the decrease in photon energy below the bandgap region. Next, Zhou et al.[61] investigated the optical properties of $GaAs_{0.979}Bi_{0.021}$ and $GaAs_{0.966}Bi_{0.034}$ p-i-n diodes using photocurrent measurement. The bandgap energies are calculated as 1.16 eV and 1.24 eV, respectively. It is also observed that α is not influenced by the depletion region, as the layers used are thin enough (350 nm and 700 nm) to assume that full depletion of the intrinsic region is achieved during the photocurrent measurement. A recent study by Liu et al.[129] discussed the behavior of α for $GaAs_{0.993}Bi_{0.007}$, $GaAs_{0.983}Bi_{0.017}$, $GaAs_{0.977}Bi_{0.023}$, $GaAs_{0.972}Bi_{0.028}$, $GaAs_{0.965}Bi_{0.035}$, $GaAs_{0.996}Bi_{0.004}$, and $GaAs_{0.94}Bi_{0.051}$ with photocurrent

measurement as illustrated in Fig. 5f. Results show that the incorporation of bismuth extends the cutoff wavelength of GaAs. At 1000 nm wavelength, the α of $GaAs_{0.965}Bi_{0.035}$ is ~ 100 times higher compared to Si. In addition, low dark current (< 10 µA) was reported for GaAsBi with 50–100 µm diameter, making GaAsBi a potential candidate for low-noise photodiodes.

Furthermore, the trend in recent work focuses on deploying new materials such as InGaAs, GaAsN, and GaAsBi with better electrical and optical performance for solar and other optoelectronics applications. Therefore, future research should focus on characterizing and calculating the optical behavior of the new ternary materials. Based on the literature review, α of ternary semiconductor materials are established. However, it would be interesting to further investigate the change in α, bandgap, and optical behavior of the material with the variation in x composition for their respective application. In addition, with reference to the α information, it is worth looking into the improvement and optimization of absorption performance for the semiconductor materials. For example, Mansur et al.[181] recently investigated the multi-variable optimization (thickness and doping concentration) of lattice-matched InGaAs using the genetic algorithm. It was found that this approach had significantly improved IR absorption and the collection of photogenerated carriers, which contributed to an improvement in TPV cell performance. This illustrates the importance of optimizing the layer thickness and doping concentration of the semiconductor materials for various applications which could be further implemented for other ternary semiconductor materials.

Quaternary Semiconductor Material

$In_{1-x}Ga_xAs_yP_{1-y}$ and $In_{1-x}Ga_xAs_ySb_{1-y}$ are common quaternary semiconductor materials that use two binary direct-bandgap materials. For example, the bandgap of $In_{1-x}Ga_xAs_yP_{1-y}$ can be engineered between 0.73 eV and 1.34 eV, often grown on InP substrate.[120] It is crucial for the α of InGaAsP to be measured accurately to improve precision in device tailoring.[76] Similarly, the x and y composition of $In_{1-x}Ga_xAs_ySb_{1-y}$ is modified to form a bandgap that varies between 0.28 eV and 0.73 eV. The ability to form different bandgaps affords high potential for various applications such as detectors, lasers, modulators, and energy harvesters and photodetectors in the near-infrared region.[149,182] To illustrate, InGaAsSb lattice-matched to GaSb is of particular interest for waste heat harvesting in low-temperature radiation.[183] The wide α range up to a wavelength of 4300 nm makes it a suitable candidate for environmental monitoring and gas analysis applications.[122]

Regarding InGaAsP absorption, Emziane et al.[66] studied the α behavior of InGaAsP (1.0 eV and 1.2 eV) lattice matched on InP with respective cutoff wavelengths at 1240 nm and 1033 nm. The α data were interpolated based on lattice-matched InGaAs, with the assumption that there is no surface recombination. Recently, Seifert et al.[120] measured the α of $In_{0.58}Ga_{0.42}As_{0.90}P_{0.1}$ (0.799 eV), $In_{0.62}Ga_{0.38}As_{0.79}P_{0.21}$ (0.857 eV), $In_{0.68}Ga_{0.32}As_{0.69}P_{0.31}$ (0.91 eV), $In_{0.81}Ga_{0.19}As_{0.42}P_{0.0.58}$ (1.062 eV) and $In_{0.89}Ga_{0.11}As_{0.24}P_{0.76}$ (1.17 eV) using the SE method. The findings are beneficial for interpolating the α of InGaAsP with other x and y composition in future work.[73] Figure 6a and b highlight the absorption coefficient curves of InGaAsP and InGaAsSb, respectively, recorded by various methods.

On the other hand, InGaAsSb has a significantly wider α spectrum than InGaAsP because the former material possesses InSb properties. In an earlier work, Peng et al.[182,184] performed numerical analysis on $In_{0.10}Ga_{0.90}As_{0.09}Sb_{0.91}$ (0.6 eV), $In_{0.12}Ga_{0.88}As_{0.10}Sb_{0.90}$ (0.58 eV), $In_{0.16}Ga_{0.84}As_{0.14}Sb_{0.86}$ (0.53 eV), and $In_{0.20}Ga_{0.80}As_{0.18}Sb_{0.82}$ (0.53 eV) using Adachi's model. The effect of cell temperature on α was also discussed for the first time. Similarly, Gonzalez-Cuevas et al.[75] numerically interpolated the α of $In_{0.14}Ga_{0.86}As_{0.14}Sb_{0.86.}$ On the other hand, the α values for $In_{0.23}Ga_{0.77}As_{0.21}Sb_{0.79}$ and $In_{0.\ 30}Ga_{0.70}As_{0.273}Sb_{0.727}$ for 2000–2800 nm high-frequency application were calculated using the SE method.[122] Previous work from Muñoz et al.[121] measured the α of $In_{0.14}Ga_{0.86}As_{0.14}Sb_{0.86}$ using the SE method, and the reported work is in good agreement with the result obtained from linear interpolation using the endpoint material. Zhang et al.[74] interpolated α for $In_{0.15}Ga_{0.85}As_{0.15}Sb_{0.85}$ with novel x and y composition for InGaAsSb for TPV application. In addition, Mitsuhara et al.[185] recently measured the α of $In_{0.65}Ga_{0.35}As_{0.90}Sb_{0.10}$. It is worth noting that α is extended to 2200 nm for a multi-quantum well structure grown on InP substrate. This is a breakthrough, as it is challenging to grow a multi-quantum well structure that manages to absorb at wavelengths beyond 2000 nm.

Next, $Ga_{1-y}In_yAs_{1-x}N_x$ with bandgap of 1–1.4 eV grown on GaAs substrate has received attention due to the effect of nitrogen in the structure towards the changes in electrical and optical properties.[102] The α information of GaInAsN is important for model the quantum efficiency behavior. It is reported that factors such as the doping concentration, bandgap, annealing process, and growth condition influence α of GaInAsN near the band edge region. The α properties of GaInAsN are similar to GaAs above the band edge region.[186] In 1998, a pioneering research work on α of $Ga_{0.92}In_{0.08}As_{0.97}N_{0.03}$ (1 eV bandgap) was conducted by using the T method.[187] With 3% of nitrogen and p-type doping concentration of 1×10^{17} cm^{-3}, an absorption value of 10,000 cm^{-1} was recorded at 1000 nm before the band edge. Also, Kurtz et al.[131] conducted research on α of $Ga_{0.93}In_{0.07}As_{0.98}N_{0.02}$ using the photocurrent method for solar cell application with > 70%

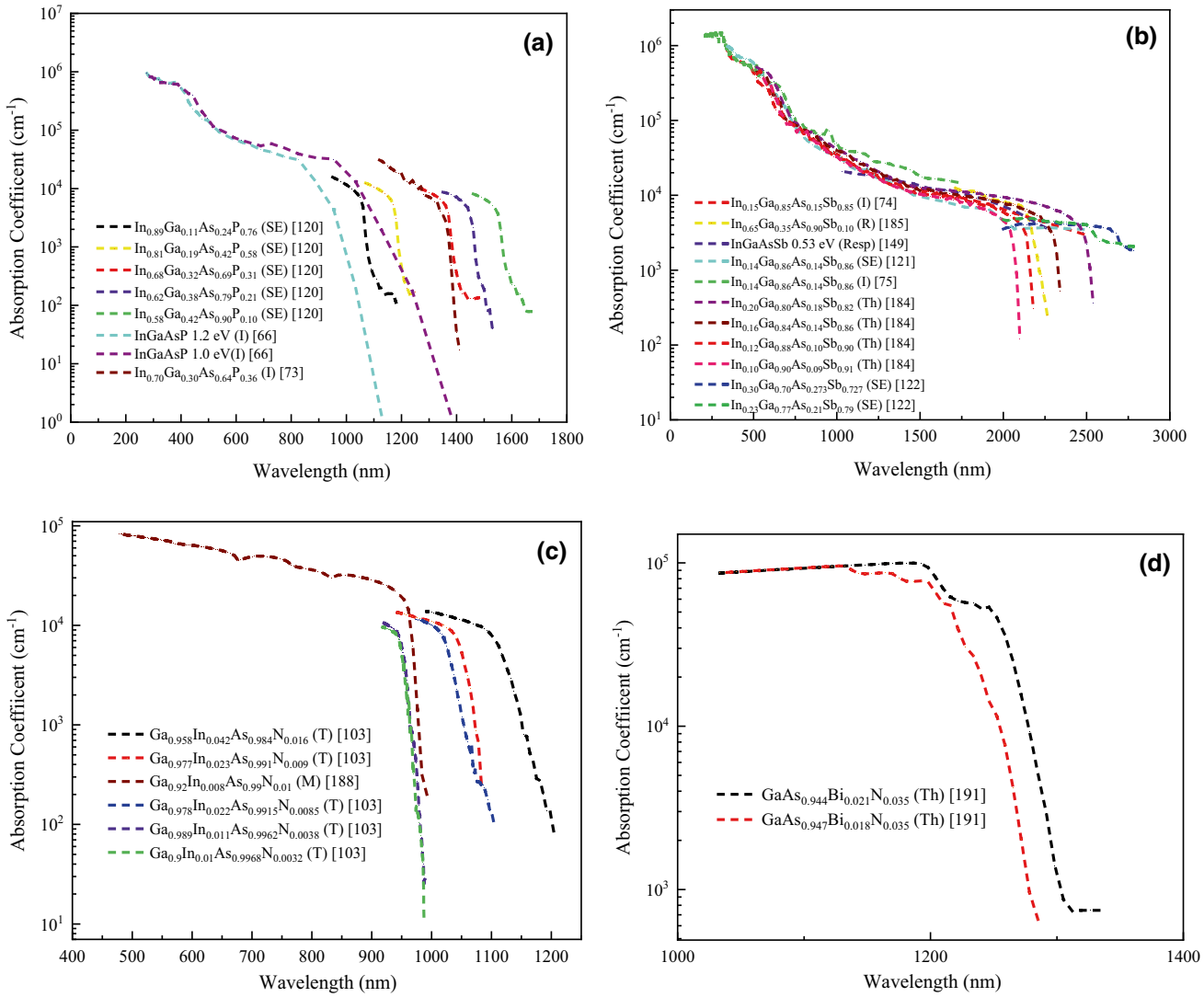

Fig. 6 Methods to calculate the α for (a) InGaAsP, (b) InGaAsSb, (c) GaInAsN, and (d) GaAsBiN.

of quantum efficiency. The α of $Ga_{0.92}In_{0.008}As_{0.99}N_{0.001}$ was calculated using Green's functions, and the transition in valence and conduction bands was observed at 700 nm and 830 nm as shown in Fig. 6c.[188] Later on, α of $Ga_{0.958}In_{0.042}As_{0.984}N_{0.016}$, $Ga_{0.977}In_{0.023}As_{0.991}N_{0.009}$, $Ga_{0.978}In_{0.022}As_{0.9915}N_{0.0085}$, $Ga_{0.989}In_{0.011}As_{0.9962}N_{0.0038}$, $Ga_{0.99}In_{0.01}As_{0.9968}N_{0.0032}$ was measured using the T method.[103] It is observed that as the ratio of nitrogen to arsenic decreases, α increases in a more rapid manner and later starts to saturate when the nitrogen composition is higher than 0.009. It is also reported that the absorption value in $Ga_{1-y}In_yAs_{1-x}N_x$ is higher compared to GaAsN with the same nitrogen ratio which is caused by the diversity of chemical environment in $Ga_{1-y}In_yAs_{1-x}N_x$.[103]

The performance of $GaAs_{1-x-y}N_xBi_y$ below 1.42 eV bandgap appears to be interesting as other narrow bandgap semiconductor materials such as InAs, GaSb, and InP are reported to have intrinsic limitations such as Auger recombination and optical loss for near- and mid-infrared application.[189] The electrical and optical properties of $GaAs_{1-x-y}N_xBi_y$ have the flexibility to be tailored in a wide range by tuning the nitrogen and bismuth composition which could be useful for optoelectronics, photonics devices and multijunction solar cell applications.[190] GaAsBiN can be grown latticed-matched on Ge and GaAs which makes it a cost-effective candidate for solar cell application. The theoretical α values of $GaAs_{0.944}N_{0.035}Bi_{0.021}$ and $GaAs_{0.947}N_{0.035}Bi_{0.018}$ were then studied as shown in Fig. 6d.[191] It is observed that when nitrogen is constant at 3.5%, the increase in bismuth from 1.8% to 2.1% contributes to the increase in cutoff wavelength (1127 nm to 1200 nm) near the infrared and telecommunication wavelength at 1300 nm. In addition, Wang et al.[192] highlighted that a small percentage of nitrogen content causes a large

reduction shift in the conduction band edge, while bismuth content contributes to an upward shift in the valence band edge. Nevertheless, previous studies have focused on the lattice constant and band structure of the device; the absorption coefficient of GaAsBiN with respect to the variation of nitrogen and bismuth content could be further studied in a more thorough manner.[193]

In summary, α of quaternary material is commonly measured using the SE method or numerically calculated using the interpolation method. Research works have focused on interpolating the absorption and roll-off trend at the bandgap for materials with variations in x and y composition. Further research is needed to investigate and measure α at different x and y composition and to develop improved methods to determine the α of InGaAsP and InGaAsSb with higher accuracy with respect to the material structure. Understanding the absorption properties of the materials is important due to their optical properties for their desired field of application.

Future Prospects and Recommendation

Semiconductor materials with cutoff wavelengths ≤ 2.0 µm have been highly developed with good state-of-the-art performance. Nevertheless, materials with cutoff wavelengths > 2.0 µm generally suffer from high dark current and noise, and these appear to be significant limitations of semiconductor materials. Exploring the absorption coefficient of new semiconductor materials in the cutoff wavelength ranging between 2.0 µm and 3.0 µm to improve the material performance with minimal optical loss is of particular interest for various applications such as infrared cameras, photodetectors, PV and TPV applications. For example, in photodetectors, an accurate electro-optical model helps tune the spectral response resulting in better device performance. Furthermore, full knowledge of the absorption coefficient and the ultrasmall absorption value is significant to optimize the performance of organic semiconductor-based solar cells[6] and ternary and quaternary semiconductor materials for mid- and far-infrared applications.

To further illustrate the importance of semiconductor materials with cutoff wavelengths ranging between 2.0 µm and 3.0 µm, TPV cells harvest waste heat for temperatures ranging from 800 K to 2000 K, which requires narrow bandgap materials such as $In_{1-x}Ga_xAs$ and $In_{1-x}Ga_xAs_ySb_{1-y}$ to convert the infrared radiation. It is worth noting that research work has been focusing on growing lattice-mismatched $In_{1-x}Ga_xAs$ and $In_{1-x}Ga_xAs_ySb_{1-y}$ at long cutoff wavelengths for TPV application. However, the absorption coefficients of the materials are not well reported. More often, the absorption coefficients of these two materials are commonly calculated using interpolation by estimating α with respect to the component ratio. The photocurrent method with EQE calculation is recommended in this case such that the mathematical equations can solve for the accurate absorption coefficient based on the device structure and photocurrent measurement. Moreover, the complexity in solving the mathematical model has appeared to be one of the constraints as there are several design parameters involved, such as $L_{e,h}$, $S_{e,h}$, and $D_{e,h}$. In this case, the introduction of artificial intelligence-based techniques such as GA appears to be a feasible approach for accurately calculating the absorption coefficient, considering the complexity of the equations and parameters involved. Another advantage of deriving α using the photocurrent measurement with advanced computation is the capability of providing detailed information at the absorption tail (Urbach Tail), which can be extrapolated to extract the bandgap value of the material. Therefore, the incorporation of intelligent computation into the photocurrent method should be further developed as a powerful tool to provide more thorough information of α for the semiconductor materials.

Based on critical literature review, transmission and reflectance methods are preferred to solve for the absorption coefficient of established materials which are grown on substrate of the same material. Nevertheless, handling the heterojunction structures, this study revealed that measurement methods such as SE, transmission and reflectance measurement have constraint in solving for the absorption coefficient data in the short wavelength region. For example, for InGaAs material with InAsP layers (as the top capping layer), the absorption coefficient of InGaAs can only be determined for wavelengths ≥ 1.3 µm due to the cutoff wavelength of InAsP at ≈ 1.3 µm. Such a scenario fails to portray the complete information of InGaAs absorption coefficient in the short wavelength region. In addition, lattice-mismatched InGaAs grown on InP substrate has several InAsP buffer layers with a variation of arsenide and phosphorous composition ratio to improve the junction performance by minimizing the defect propagation from the substrate or the InGaAs growth interface. The cutoff wavelengths of the buffer layers vary according to the InAsP composition, and the strain in buffer layer would cause the shift in bandgap. Hence, the absorption coefficient of InGaAs would not be accurately measured by SE, transmission or reflectance. Focusing on the future characterization work of new ternary and quaternary compounds grown on a low-cost substrate, transmission and reflectance can be used as an initial check on the range of α. However, to accurately determine the α of the material, the photocurrent method would comparatively be the more feasible method as the measurement eliminates the effects of buffer layers and the calculation takes into account detailed information of $L_{e(h)}$, $S_{e(h)}$, and $D_{e(h)}$ of the material composition. In this case, it is recommended to incorporate GA with the ability to handle the complexity

of photocurrent measurement and calculation to solve the detailed information of α.

Of the numerous experimental measurements and mathematical models for α of semiconductor materials reviewed, experimental measurement has limitations in terms of accuracy and consistency, especially when handling devices with uneven surfaces or nonuniformity across a single wafer. At the same time, interpolation provides an estimation of α for new ternary and quaternary materials. This method provides a predictive analysis of the ternary and quaternary material's optical properties solely based on the material composition, without considering the electrical properties of the structure design. With reference to the collected α data of single element, binary, ternary, and quaternary materials, it is recommended that the collected data are fed into an artificial neural network (ANN) algorithm as a novel intelligent method to solve for α for the new semiconductor material. This can be made practical in the scenario where the contributing design parameters that lead to the variation of α are very clearly defined and identified. For example, the bandgap and other material parameters, such as the diffusion length and surface recombination velocity, must be identified as the input parameters with respect to α. Based on the input database of various semiconductors, the ANN can be trained intelligently to solve for α of any new semiconductor material. This approach would be beneficial for the new composition of ternary and quaternary semiconductor materials. In addition, the results would be more accurate compared to the interpolation method, as the details of the semiconductor device parameters will be taken into account for the predictive analysis. Most importantly, such a breakthrough in α research would be beneficial and cost-efficient compared to the experimental measurement.

In addition, future work could further investigate the absorption coefficient of the new ternary and quaternary semiconductor materials and look into the feasibility of methods and advancements in technology to grow them on large-area and low-cost substrates such as Si, InP, Ge, GaAs, and GaSb for large-scale production. For example, InGaAsSb has been identified to be more cost-effective when it is grown on a GaAs substrate compared to InGaAsSb grown lattice-matched on a GaSb substrate.[59] Thus, the breakthrough in overcoming the cost factor in the growth process would significantly increase the opportunity for commercialization. Additionally, new quaternary materials such as AlGaAsSb and AlInAsSb photodiodes grown on InP substrate have recently received tremendous attention to be commercialized owing to their economical substrate cost and low noise advantages.[194]

It is also essential to increase the absorbance of the materials to improve the overall performance efficiency. Several loss factors decrease the likelihood of absorbance in the designed structures. For example, the refractive index of air on Si causes a reflection of approximately 35% of the total incident photons, decreasing the beam intensity and output performance, especially for photovoltaic applications. Significant absorption improvement can be obtained by applying an optimum anti-reflective coating and texturing the front cell surface.[195] To illustrate, it is recommended that semiconductor devices made of materials such as InGaAs, Ge and InGaAsSb, are designed with anti-reflective coating material such as MgO_2 or TiO_2 to improve the absorption of the cell material, hence improving the power harvesting system efficiency. Furthermore, optical losses occur significantly through transmission distance. Therefore, penetration length of material must be designed carefully to avoid transmission loss.[196] To reduce optical transmission losses, mechanisms such as texturing the back surface reflector and air bridge are implemented to trap light and increase the transmission path.[197] Similarly, it is suggested that back surface reflector material could be further developed and utilized to improve the performance of power harvesting applications. Additionally, engineering ohmic metamaterial with transparent properties and high conductivity will reduce the optical and electrical losses and hence improve the absorbance. These factors will assist in improving the performance of various semiconductor devices for the targeted applications.

Conclusion

Accurate absorption coefficient information of the semiconductor material is crucial in designing various semiconductor devices. This paper has presented a comprehensive analysis of the mathematical derivation of different methods to numerically solve and measure α for semiconductor materials, highlighting the accuracy of the respective method, advantages and disadvantages followed by potential recommendations. In addition, this paper comprehensively summarized the α data of various single-element, binary, ternary and quaternary semiconductor materials with the discussion of the fundamental optical properties and recent studies in optimizing the optical performance. In general, α of single-element and binary semiconductor materials is mainly identified using optical and electrical methods. The measurement results are consistent and well-established, yet future work could focus on improving the absorption performance using anti-reflective coating and structure optimization. In contrast, the absorption coefficient of ternary and quaternary semiconductor materials correspond to the various measurement methods are not thoroughly reported. The α of new ternary and quaternary material in the long cutoff wavelength is worth further investigation for optoelectronics, photodetectors, and heat harvesting applications.

Lastly, the review has articulated the advancement of using artificial methods such as GA and ANN to accurately determine α based on the detailed information of material structure. These novel methods can trigger a simple yet effective approach to obtain the α of semiconductors and are favorable for both new and available ternary and quaternary materials for the mid- and long-IR region.

Acknowledgments This work was supported by the Tenaga Nasional Berhad Seeding Fund that is managed by UNITEN R&D Sdn. Bhd. with the project code: U-TG-RD-18-04 and UNITEN BOLD grant J510050002/2022019.

Conflict of interest The authors declare that they have no conflict of interest.

References

1. A. Gitelson, A. Viña, A. Solovchenko, T. Arkebauer, and Y. Inoue, Derivation of Canopy Light Absorption Coefficient from Reflectance Spectra. *Remote Sens. Environ.* 231, 111276 (2019).
2. S. Zhou, L. Xu, K. Chen, L. Zhang, B. Yu, T. Jiang, and J. Li, Absorption Spectroscopy Gas Sensor Using a Low-Cost Quartz Crystal Tuning Fork with an Ultrathin Iron Doped Cobaltous Oxide Coating. *Sens. Actuators B Chem.* 326, 128951 (2021).
3. J. Treu, X. Xu, K. Ott, K. Saller, G. Abstreiter, J.J. Finley, and G. Koblmüller, Optical Absorption of Composition-Tunable InGaAs Nanowire Arrays. *Nanotechnology* 30, 495703 (2019).
4. A. Sergeev, S. Karnani, and C.M. Waits, Modeling TPV Devices Based on Exact Analytical Solution of the Generalized Shockley-Queisser Model. *MRS Adv.* 4, 905 (2019).
5. J.S. Cheong, J.S. Ng, A.B. Krysa, J.S.L. Ong, and J.P.R. David, Determination of Absorption Coefficients in AlInP Lattice Matched to GaAs. *J. Phys. D. Appl. Phys.* 48, 405101 (2015).
6. C. Kaiser, S. Zeiske, P. Meredith, and A. Armin, Determining Ultralow Absorption Coefficients of Organic Semiconductors from the Sub-Bandgap Photovoltaic External Quantum Efficiency. *Adv. Opt. Mater.* 8, 1 (2020).
7. H. Son, D.-H. Choi, and G.-S. Park, Improved Thickness Estimation of Liquid Water Using Kramers-Kronig Relations for Determination of Precise Optical Parameters in Terahertz Transmission Spectroscopy. *Opt. Express* 25, 4509 (2017).
8. G. Rey, C. Spindler, F. Babbe, W. Rachad, and S. Siebentritt, Absorption Coefficient of a Semiconductor Thin Film from Photoluminescence. *Am. Phys. Soc.* 9, 064008 (2018).
9. Y. Jin, B. Song, Z. Jia, Y. Zhang, C. Lin, X. Wang, and S. Dai, Improvement of Swanepoel Method for Deriving the Thickness and the Optical Properties of Chalcogenide Thin Films. *Opt. Express* 25, 440 (2017).
10. C. Schinke, P. Christian Peest, J. Schmidt, R. Brendel, K. Bothe, M.R. Vogt, I. Kröger, S. Winter, A. Schirmacher, S. Lim, H.T. Nguyen, and D. Macdonald, Uncertainty Analysis for the Coefficient of Band-to-Band Absorption of Crystalline Silicon. *AIP Adv.* 5, 067168 (2015).
11. E. Vadiee, Y. Fang, C. Zhang, A.M. Fischer, J.J. Williams, E.J. Renteria, G. Balakrishnan, and C.B. Honsberg, Temperature Dependence of GaSb and AlGaSb Solar Cells. *Curr. Appl. Phys.* 18, 752 (2018).
12. C. Howlader, M. Hasan, A. Zakhidov, and M.Y. Chen, Determining the Refractive Index and the Dielectric Constant of PPDT2FBT Thin Film Using Spectroscopic Ellipsometry. *Opt. Mater. (Amst.)* 110, 110445 (2020).
13. M. De Kersauson, R. Jakomin, M. El Kurdi, G. Beaudoin, N. Zerounian, F. Aniel, S. Sauvage, I. Sagnes, and P. Boucaud, Direct and Indirect Band Gap Room Temperature Electroluminescence of Ge Diodes. *J. Appl. Phys.* 108, 023105 (2010).
14. X. Li, T. Wang, W. Yan, C. Dong, and J. Tang, Direct and Indirect Intraband Optical Absorption Due to Carrier Transitions from Discrete Levels to Continuum States in Quantum Dot System. *Appl. Phys. Lett.* 102, 113512 (2013).
15. J.A. Polo, T.G. Mackay, and A. Lakhtakia, Surface-plasmon-polariton waves I, in *Electromagnetic Surface Waves* (Elsevier, 2013), pp. 37–80.
16. G. Yu, G. Wang, H. Ishikawa, M. Umeno, T. Soga, T. Egawa, J. Watanabe, and T. Jimbo, Optical Properties of Wurtzite Structure GaN on Sapphire around Fundamental Absorption Edge (0.78–4.77 EV) by Spectroscopic Ellipsometry and the Optical Transmission Method. *Appl. Phys. Lett.* 70, 3209 (1997).
17. G.G. Macfarlane and V. Roberts, Infrared Absorption of Germanium near the Lattice Edge [2]. *Phys. Rev.* 97, 1714 (1955).
18. D. Poelman and P.F. Smet, Methods for the Determination of the Optical Constants of Thin Films from Single Transmission Measurements: A Critical Review. *J. Phys. D. Appl. Phys.* 36, 1850 (2003).
19. R. Swanepoel, Determination of the Thickness and Optical Constants of Amorphous Silicon. *J. Phys. E.* 16, 1214 (1983).
20. K.A. Aly, N. Afify, A.M. Abousehlly, and A.M. Abd Elnaeim, Optical Band Gap and Refractive Index Dispersion Parameters of In-Se-Te Amorphous Films. *J. Non-Cryst. Solids* 357, 2029 (2011).
21. D. Dorranian, L. Dejam, and G. Mosayebian, Optical Characterization of Cu_3N Thin Film with Swanepoel Method. *J. Theor. Appl. Phys.* 6, 13 (2012).
22. R. Yavorskyi, L. Nykyruy, G. Wisz, P. Potera, S. Adamiak, and S. Górny, Structural and Optical Properties of Cadmium Telluride Obtained by Physical Vapor Deposition Technique. *Appl. Nanosci.* 9, 715 (2019).
23. M.H. Saleh, N.M. Ershaidat, M.J. Ahmad, B.N. Bulos, and M.M. Jafar, Evaluation of Spectral Dispersion of Optical Constants of A-Se Films from Their Normal-Incidence Transmittance Spectra Using Swanepoel Algebraic Envelope Approach. *Opt. Rev.* 24, 260 (2017).
24. J. Yang, Y. Gao, Z. Huang, X. Meng, M. Shen, H. Yin, J. Sun, and J. Chu, Dielectric Functions of Ferroelectric $Pb_{0.5}Sr_{0.5}TiO_3$ Film Determined by Transmittance Spectroscopy. *J. Phys. D. Appl. Phys.* 42, 215403 (2009).
25. A. Ganjoo and R. Golovchak, Computer Program PARAV for Calculating Optical Constants of Thin Films and Bulk Materials: Case Study of Amorphous Semiconductors. *J. Optoelectron. Adv. Mater.* 10, 1328 (2008).
26. S. Jena, R.B. Tokas, S. Thakur, and D.V. Udupa, PRISA: A Simple Software for Determining Refractive Index, Extinction Co-Efficient, Dispersion Energy, Band Gap, and Thickness of Semiconductor and Dielectric Thin Films. arXiv (2020).
27. D.S. Gerber and G.N. Maracas, A Simple Method for Extraction of Multiple Quantum Well Absorption Coefficient from Reflectance and Transmittance Measurements. *IEEE J. Quantum Electron.* 29, 2589 (1993).
28. J. Strong, *Procedures in Experimental Physics*, 1st ed., (New York: Prentice-Hall, 1938).
29. M. Becker and H.Y. Fan, Optical Properties of Semiconductors. III. Infra-Red Transmission of Silicon. *Phys. Rev.* 76, 1531 (1949).
30. R.B. Barnes and M. Czerny, Concerning The Reflection Power of Metals in Thin Layers for the Infrared. *Phys. Rev.* 38, 338 (1931).

31. S. Wojtczuk, P. Colter, G. Charache, and D. DePoy, Performance Status of 0.55eV InGaAs Thermophotovoltaic Cells, in *Thermophotovoltaic Generation of Electricity: Fourth NREL Conference*, vol. 417 (2011), pp. 417–426.
32. C.H. Huang, G. Zhang, Z.Q. Chen, X.J. Huang, and H.Y. Shen, Calculation of the Absorption Coefficients of Optical Materials by Measuring the Transmissivities and Refractive Indices. *Opt. Laser Technol.* 34, 209 (2002).
33. J. Menéndez, D.J. Lockwood, J.C. Zwinkels, and M. Noël, Phonon-Assisted Optical Absorption in Germanium. *Phys. Rev. B* 98, 165207 (2018).
34. T. Zhan, X. Shi, Y. Dai, X. Liu, and J. Zi, Transfer Matrix Method for Optics in Graphene Layers. *J. Phys. Condens. Matter* 25, 215301 (2012).
35. G. Ariyawansa, E. Steenbergen, L.J. Bissell, J.M. Duran, J.E. Scheihing, and M.T. Eismann, Absorption Characteristics of Mid-Wave Infrared Type-II Superlattices. *Infrared Technol. Appl. XL* 9070, 90701J (2014).
36. O. Guasch, P. Sánchez-Martín, and D. Ghilardi, Application of the Transfer Matrix Approximation for Wave Propagation in a Metafluid Representing an Acoustic Black Hole Duct Termination. *Appl. Math. Model.* 77, 1881 (2020).
37. S.H. Wemple and J.A. Seman, Optical Transmission Through Multilayered Structures. *Appl. Opt.* 12, 2947 (1973).
38. J.F. Muth, J.H. Lee, I.K. Shmagin, R.M. Kolbas, H.C. Casey, B.P. Keller, U.K. Mishra, and S.P. DenBaars, Absorption Coefficient, Energy Gap, Exciton Binding Energy, and Recombination Lifetime of GaN Obtained from Transmission Measurements. *Appl. Phys. Lett.* 71, 2572 (1997).
39. N. Jiménez, J.P. Groby, V. Pagneux, and V. Romero-García, Iridescent Perfect Absorption in Critically-Coupled Acoustic Metamaterials Using the Transfer Matrix Method. *Appl. Sci.* 7, 618 (2017).
40. L. Zhang, S.A. Ding, and G. Qin, Efficiency Simulations on Perovskite Solar Cells Only Using Experimentally Determined Reflectance and Transmittance Data. *Sol. Energy Mater. Sol. Cells* 201, 110039 (2019).
41. D.H. Lee and Y.P. Kwon, Estimation of the Absorption Performance of Multiple Layer Perforated Panel Systems by Transfer Matrix Method. *J. Sound Vib.* 278, 847 (2004).
42. C.M. Lee and Y. Xu, A Modified Transfer Matrix Method for Prediction of Transmission Loss of Multilayer Acoustic Materials. *J. Sound Vib.* 326, 290 (2009).
43. C.C. Katsidis and D.I. Siapkas, Systems With Coherent, Partially Coherent, and Incoherent Interference. *Appl. Opt.* 41, 3978 (2002).
44. X.H. Deng, J.T. Liu, J.R. Yuan, Q.H. Liao, and N.H. Liu, A New Transfer Matrix Method to Calculate the Optical Absorption of Graphene at Any Position in Stratified Media. *EPL* 109, 27002 (2015).
45. U. R. I. Virgili, C. Of, P. Silicon, and M. Optical, *Chapter 3: Simulation Programs for the Analysis of Multilayer Media* (2007).
46. E. Daub and P. Würfel, Ultralow Values of the Absorption Coefficient of Si Obtained from Luminescence. *Phys. Rev. Lett.* 74, 1020 (1995).
47. P. Drude, *The Theory of Optics* (London: Longmans, Green & Co., 1922).
48. L.R. Ingersoll and J.T. Littleton Jr., A New Method of Determining the Optical Constants of Metals, and the Optical Constants of Silicon. *Phys. Rev.* 31, 489 (1910).
49. R.W.U. Collins, I. An, H. Fujiwara, J. Lee, Y. Lu, J. Koh, and P.I. Rovira, Advances in Multichannel Spectroscopic Ellipsometry. *Thin Solid Films* 313–314, 18 (1998).
50. H. Kato, S. Adachi, H. Nakanishi, and K. Ohtsuka, Optical Properties of $(Al_xGa_{1-x})_{0.5}In_{0.5}P$ Quaternary Alloys. *Jpn. J. Appl. Phys.* 33, 186 (1994).
51. F. Abdel-Wahab, I.M. Ashraf, and A.A. Montaser, Spectroscopic Ellipsometry Study of TlGaSeS Layered Crystal. *Optik (Stuttg)* 178, 813 (2019).
52. A. Roseler and E.-H. Korte, Infrared spectroscopic ellipsometry, *Handbook of Vibrational Spectroscopy*. ed. J.M. Chalmers (Chichester: Wiley, 2006).
53. L.Q. Zhu, Q. Fang, G. He, M. Liu, X.X. Xu, and L.D. Zhang, Spectroscopic Ellipsometry Characterization of ZrO_2 Thin Films by Nitrogen-Assisted Reactive Magnetron Sputtering. *Mater. Sci. Semicond. Process.* 9, 1025 (2006).
54. E.A. Irene, Applications of Spectroscopic Ellipsometry to Microelectronics. *Thin Solid Films* 233, 96 (1993).
55. V.G. Kravets, A.N. Grigorenko, R.R. Nair, P. Blake, S. Anissimova, K.S. Novoselov, and A.K. Geim, Spectroscopic Ellipsometry of Graphene and an Exciton-Shifted van Hove Peak in Absorption. *Phys. Rev. B Condens. Matter Mater. Phys.* 81, 155413 (2010).
56. J. Humlíček, 1: Polarized light and ellipsometry, *Handbook of Ellipsometry*. ed. H.G. Tompkins, and E.A. Irene (Norwich: William Andrew Publishing, 2005), pp. 3–91.
57. N.S. Samarasingha, S. Zollner, D. Pal, R. Singh, and S. Chattopadhyay, Thickness Dependence of Infrared Lattice Absorption and Excitonic Absorption in ZnO Layers on Si and SiO_2 Grown by Atomic Layer Deposition. *J. Vac. Sci. Technol. B* 38, 042201 (2020).
58. E. Papis, A. Kudla, T.T. Piotrowski, K. Golaszewska, E. Kamińska, and A. Piotrowska, Ellipsometric Investigations of (1 0 0) GaSb Surface under Chemical Etching and Sulfide Treatment. *Mater. Sci. Semicond. Process.* 4, 293 (2001).
59. Q. Lu, A. Marshall, and A. Krier, Metamorphic Integration of GaInAsSb Material on GaAs Substrates for Light Emitting Device Applications. *Materials (Basel)* 12, 1743 (2019).
60. Q. Lu, R. Beanland, D. Montesdeoca, P.J. Carrington, A. Marshall, and A. Krier, Low Bandgap GaInAsSb Thermophotovoltaic Cells on GaAs Substrate with Advanced Metamorphic Buffer Layer. *Sol. Energy Mater. Sol. Cells* 191, 406 (2019).
61. Z. Zhou, D.F. Mendes, R.D. Richards, F. Bastiman, and J.P. David, Absorption Properties of GaAsBi Based P-i-n Heterojunction Diodes. *Semicond. Sci. Technol.* 30, 94004 (2015).
62. C.J. Hunter, F. Bastiman, A.R. Mohmad, R. Richards, J.S. Ng, S.J. Sweeney, and J.P.R. David, Absorption Characteristics of $GaAs_{1-X}$ Bi_x/GaAs Diodes in the Near-Infrared. *IEEE Photonics Technol. Lett.* 24, 2191 (2012).
63. J. Tauc, Optical properties of amorphous semiconductors, in *Amorphous and Liquid Semiconductors* (Springer, Boston, 1974), pp. 159–220.
64. M.I. Yernaux, C. Battochio, P. Verlinden, and F. Van De Wiele, A One-Dimensional Model for the Quantum Efficiency of Front-Surface-Field Solar Cells. *Sol. Cells* 13, 83 (1984).
65. G.P. Donati, R. Kaspi, and K.J. Malloy, Interpolating Semiconductor Alloy Parameters: Application to Quaternary III-V Band Gaps. *J. Appl. Phys.* 94, 5814 (2003).
66. M. Emziane and R.J. Nicholas, Optimization of InGaAs(P) Photovoltaic Cells Lattice Matched to InP. *Am. Inst. Phys.* 101, 054503 (2007).
67. R.S. Tuley and R.J. Nicholas, Material Parameters and Device Optimization : Supplementary Information for Bandgap Dependent Thermophotovoltaic Device Performance Using the InGaAs and InGaAsP Material System. *J. Appl. Phys.* 108, 156018 (2010).
68. M. Zierak, J.M. Borrego, I. Bhat, R.J. Gutmann, and G. Charache, Modeling of InGaSb Thermophotovoltaic Cells and Materials. *API Conf. Proc.* 55, 55 (1997).

69. *Springer Handbook of Electronic and Photonic Materials* (2017).
70. R.K. Jain, Suitability of InP window layers for InGaAs solar cells, in *Proceedings of 3rd World Conference on Photovoltaic Energy Conversion*, vol. 1 (2003), p. 75.
71. T.F. Refaat, M. Nurul Abedin, V. Bhagwat, I.B. Bhat, P.S. Dutta, and U.N. Singh, InGaSb Photodetectors Using an InGaSb Substrate for 2 Mm Applications. *Appl. Phys. Lett.* 85, 1874 (2004).
72. L. Zhu, Y. Hazama, A. Reddy, K. Watanabe, Y. Nakano, M. Sugiyama, and H. Akiyama, Modeling and Design for Low-Cost Multijunction Solar Cell via Light-Trapping Rear Texture Technique: Applied in InGaP/GaAs/InGaAs Triple Junction. *Prog. Photovoltaics Res. Appl.* 28, 251 (2020).
73. M. Ohring and L. Kasprzak, *An Overview of Electronic Devices and Their Reliability* (Cambridge: Academic Press, 2015).
74. X.L. Zhang, A.B. Huang, Y.Y. Lou, X. Li, M. Cui, and Y. Wang, Thermophotovoltaic Energy Conversion with GaSb Lattice-Matched $Ga_xIn_{1-x}As_ySb_{1-y}$ Diodes. *IEEE Trans. Electron Devices* 66, 901 (2019).
75. J.A. Gonzalez-Cuevas, T.F. Refaat, M.N. Abedin, and H.E. Elsayed-Ali, Calculations of the Temperature and Alloy Composition Effects on the Optical Properties of $Al_xGa_{1-x}As_ySb_{1-y}$ and $Ga_xIn_{1-x}As_ySb_{1-y}$ in the Spectral Range 0.5–6 EV. *J. Appl. Phys.* 102, 014504 (2007).
76. H. Burkhard, H.W. Dinges, and E. Kuphal, Optical Properties of $In_{1-X}Ga_xP_{1-Y}As_y$, InP, GaAs, and GaP Determined by Ellipsometry. *J. Appl. Phys.* 53, 655 (1982).
77. D.A. Humphreys, R.J. King, D. Jenkins, and A.J. Moseley, Measurement of Absorption Coefficients of $Ga_{0.47}In_{0.53}As$ over the Wavelength Range 1.0–1.7 Mm. *Electron. Lett.* 21, 1187 (1985).
78. F.R. Bacher, J.S. Blakemore, J.T. Ebner, and J.R. Arthur, Optical-Absorption Coefficient of $In_{1-X}Ga_xAs/InP$. *Phys. Rev. B* 37, 2551 (1988).
79. L. Zhou, Y.G. Zhang, Y. Gu, X.Y. Chen, Y.Y. Cao, and H.S.B.Y. Li, Absorption Coefficients of $In_{0.8}Ga_{0.2}As$ at Room Temperature and 77 K. *J. Alloys Compd.* 576, 336 (2013).
80. P. Schygulla, P. Fuß-Kailuweit, O. Höhn, and F. Dimroth, Determination of the Complex Refractive Index of Compound Semiconductor Alloys for Optical Device Modelling. *J. Phys. D. Appl. Phys.* 53, 495104 (2020).
81. B.T. Laboratories, M. Hill, and I.E. Results, The Optical Constants of Germanium in the Infra-Red and Visible. *Phys. Rev.* 75, 1705 (1949).
82. K.A. Aly, Optical Band Gap and Refractive Index Dispersion Parameters of $As_XSe_{70}Te_{30-x}$ ($0 \leq x \leq 30$ at.%) Amorphous Films. *Appl. Phys. A Mater. Sci. Process.* 99, 913 (2010).
83. K. Bücher, J. Bruns, and H.G. Wagemann, Absorption Coefficient of Silicon: An Assessment of Measurements and the Simulation of Temperature Variation. *J. Appl. Phys.* 75, 1127 (1994).
84. H. Wang, X. Liu, and Z.M. Zhang, Absorption Coefficients of Crystalline Silicon at Wavelengths from 500 Nm to 1000 Nm. *Int. J. Thermophys.* 34, 213 (2013).
85. G.Z. Mashanovich, C.J. Mitchell, J.S. Penades, A.Z. Khokhar, C.G. Littlejohns, W. Cao, Z. Qu, S. Stanković, F.Y. Gardes, T. Ben Masaud, H.M.H. Chong, V. Mittal, G.S. Murugan, J.S. Wilkinson, A.C. Peacock, and M. Nedeljkovic, Germanium Mid-Infrared Photonic Devices. *J. Light. Technol.* 35, 624 (2017).
86. W.J. Turner and W.E. Reese, Absorption Data of Laser-Type GaAs at 300° and 77°K. *J. Appl. Phys.* 35, 350 (1964).
87. H.C. Casey, D.D. Sell, and K.W. Wecht, Concentration Dependence of the Absorption Coefficient for N- and p-Type GaAs between 1.3 and 1.6 EV. *J. Appl. Phys.* 46, 250 (1975).
88. D.D. Sell and H.C. Casey, Optical Absorption and Photoluminescence Studies of Thin GaAs Layers in GaAs Single Bond Sign $Al_xGa_{1-X}As$ Double Heterostructures. *J. Appl. Phys.* 45, 800 (1974).
89. S. Abroug, F. Saadallah, and N. Yacoubi, Photothermal Investigations of Doping Effects on Opto-Thermal Properties of Bulk GaSb. *J. Alloys Compd.* 484, 772 (2009).
90. M.N. Abedin, T.F. Refaat, I.B. Bhat, Y. Xiao, S.V. Bandara, and S.D. Gunapala, Progress of Multicolor Single Detector to Detector Array Development for Remote Sensing. *Infrared Spaceborne Remote Sens. XII* 5543, 239 (2004).
91. J.R. Dixon and J.M. Ellis, Optical Properties of N-Type Indium Arsenide in the Fundamental Absorption Edge Region. *Phys. Rev.* 123, 1560 (1961).
92. S. Adachi, Optical Dispersion Relations for GaP, GaAs, GaSb, InP, InAs, InSb, $Al_XGa_{1-X}As$, and $In_{1-X}Ga_xAs_YP_{1-Y}$. *J. Appl. Phys.* 66, 6030 (1989).
93. D.E. Aspnes and A.A. Studna, Dielectric Functions and Optical Parameters of Si, Ge, GaP, GaAs, GaSb, InP, InAs, and InSb from 1.5 to 6.0 EV. *Phys. Rev. B* 27, 985 (1983).
94. A. Dutta, R. Sengupta, A. Krishnan, S. Islam, and N. Dhar, Broadband Detector for Optical Communication. *Act. Passiv. Opt. Components Commun. VII* 6775, 67750G (2007).
95. F. Deng, H. Cao, L. Liang, J. Li, J. Gao, H. Zhang, R. Qin, and C. Liu, Determination of the Basic Optical Parameters of $ZnSnN_2$. *Opt. Lett.* 40, 1282 (2015).
96. M. Freeman, R. Fahey, M. Timmons, J. Egley, K. Zhang, R. Dziendziel, G. Charache, D. DePoy, J. Borrego, P. Baldasaro, B. Campbell, and P. Sharps, Electrical and Optical Properties of Degenerately-Doped (2009), p. 215.
97. X.L. Zhang, A.B. Huang, C.Y. Tian, Y. Wang, and Y.Y. Lou, Thermophotovoltaic Generation of Electricity with $InAs_{0.91}Sb_{0.09}$ Device. *IEEE Trans. Electron Devices* 65, 4429 (2018).
98. G.B. Stringfellow and P.E. Greene, Liquid Phase Epitaxial Growth of $InAs_{1-x}Sb_X$. *J. Electrochem. Soc.* 118, 805 (1971).
99. W. Dobbelaere, J. De Boeck, P. Van Mieghem, R. Mertens, and G. Borghs, Optical Characterization of Si-Doped InAs1-XSbx Grown on GaAs and GaAs-Coated Si by Molecular-Beam Epitaxy. *J. Appl. Phys.* 69, 2536 (1991).
100. E. Plis, P. Rotella, S. Raghavan, L.R. Dawson, S. Krishna, D. Le, and C.P. Morath, Growth of Room-Temperature "Arsenic Free" Infrared Photovoltaic Detectors on GaSb Substrate Using Metamorphic InAlSb Digital Alloy Buffer Layers. *Appl. Phys. Lett.* 82, 1658 (2003).
101. K. Uesugi, I. Suemune, T. Hasegawa, T. Akutagawa, and T. Nakamura, Temperature Dependence of Band Gap Energies of GaAsN Alloys. *Appl. Phys. Lett.* 76, 1285 (2000).
102. S. Turcotte, J.N. Beaudry, R.A. Masut, P. Desjardins, G. Bentoumi, and R. Leonelli, Experimental Investigation of the Variation of the Absorption Coefficient with Nitrogen Content in GaAsN and GaInAsN Grown on GaAs (001). *J. Appl. Phys.* 104, 083511 (2008).
103. A. Boumesjed, H. Mazari, K. Ameur, N. Benseddik, S. Kadid, N. Benyahya, and Z. Benamara, Simulation of the GaAsN-Based Schottky Solar Cell Prototype. *Int. J. Ambient Energy* 43, 726 (2022).
104. H.R. Philipp and E.A. Taft, Optical Constants of Germanium in the Region I to 10 Ev. *Phys. Rev.* 113, 1002 (1959).
105. J.I. Pankove and P. Aigrain, Optical Absorption of Arsenic-Doped Degenerate Germanium. *Phys. Rev.* 126, 956 (1962).
106. A. Chandola, R. Pino, and P.S. Dutta, Below Bandgap Optical Absorption in Tellurium-Doped GaSb. *Semicond. Sci. Technol.* 20, 886 (2005).
107. O.G. Lorimor and W.G. Spitzer, Infrared Refractive Index and Absorption of InAs and CdTe. *J. Appl. Phys.* 36, 1841 (1965).
108. T.S. Moss, S.D. Smith, and T.D.F. Hawkins, Absorption and Dispersion of Indium Antimonide. *Proc. Phys. Soc. Sect. B* 70, 776 (1957).

109. A.R. Goni, K. Strössner, K. Syassen, and M. Cardona, Pressure Dependence of Direct and Indirect Optical Absorption in GaAs. *Phys. Rev. B* 36, 1581 (1987).
110. M. Jin, B. Chang, H. Cheng, J. Zhao, M. Yang, X. Chen, and G. Hao, Research on Quantum Efficiency of Transmission-Mode InGaAs Photocathode. *Optik (Stuttg)* 125, 2395 (2014).
111. M.A. Green and M.J. Keevers, Optical Properties of Intrinsic Silicon at 300. *Prog. Photovolt. Res. Appl.* 3, 189 (1995).
112. C.M. Herzinger, B. Johs, W.A. McGahan, J.A. Woollam, and W. Paulson, Ellipsometric Determination of Optical Constants for Silicon and Thermally Grown Silicon Dioxide via a Multi-Sample, Multi-Wavelength, Multi-Angle Investigation. *J. Appl. Phys.* 83, 3323 (1998).
113. C.Y. Tsao, P. Campbell, D. Song, and M.A. Green, Influence of Hydrogen on Structural and Optical Properties of Low Temperature Polycrystalline Ge Films Deposited by RF Magnetron Sputtering. *J. Cryst. Growth* 312, 2647 (2010).
114. M.D. Sturge, Optical Absorption of Gallium Arsenide between 0.6 and 2.75 EV. *Phys. Rev.* 127, 768 (1962).
115. M. Muñoz, K. Wei, F.H. Pollak, J.L. Freeouf, and G.W. Charache, Spectral Ellipsometry of GaSb: Experiment and Modeling. *Phys. Rev. B Condens. Matter Mater. Phys.* 60, 8105 (1999).
116. X. Zhang, Y.S. Ang, J. can Chen, and L.K. Ang, Design of an InSb Thermoradiative System for Harvesting Low-Grade Waste Heat. *Opt. Lett.* 44, 3354 (2019).
117. V.R. D'Costa, K.H. Tan, B.W. Jia, S.F. Yoon, and Y.C. Yeo, Mid-Infrared to Ultraviolet Optical Properties of InSb Grown on GaAs by Molecular Beam Epitaxy. *J. Appl. Phys.* 117, 1 (2015).
118. M.A. Marciniak, R.L. Hengehold, Y.K. Yeo, and G.W. Turner, Optical Characterization of Molecular Beam Epitaxially Grown InAsSb Nearly Lattice Matched to GaSb. *J. Appl. Phys.* 84, 480 (1998).
119. Y. Sun, K.H. Montgomery, X. Wang, S. Tomasulo, M.L. Lee, and P. Bermel, Modeling wide bandgap GaInP photovoltaic cells for conversion efficiencies up to 16.5%, in *IEEE 42nd Photovoltaic Specialist Conference (PVSC)* (2015).
120. S. Seifert and P. Runge, Revised Refractive Index and Absorption of $In_{1-x}Ga_xAs_yP_{1-y}$ Lattice-Matched to InP in Transparent and Absorption IR-Region. *Opt. Mater. Express* 6, 629 (2016).
121. M. Muñoz, K. Wei, F.H. Pollak, J.L. Freeouf, C.A. Wang, and G.W. Charache, Optical Constants of $Ga_{1-x}In_xAs_ySb_{1-y}$ lattice Matched to Gasb (001): Experiment and Modeling. *J. Appl. Phys.* 87, 1780 (2000).
122. B. Liang, D. Chen, B. Wang, T.A. Kwasniewski, and Z. Wang, Analysis, Optimization, and Design of 2–2.8 Mm Stacked Multiple-Junction PIN GaInAsSb/GaSb Photodetectors for Future O/E Interconnections. *IEEE Trans. Electron Devices* 57, 361 (2010).
123. Q. Lu, X. Zhou, A. Krysa, A. Marshall, P. Carrington, C.H. Tan, and A. Krier, InAs Thermophotovoltaic Cells with High Quantum Efficiency for Waste Heat Recovery Applications Below 1000 °C. *Sol. Energy Mater. Sol. Cells* 179, 334 (2018).
124. L.W. Lim, C.H. Tan, J.S. Ng, J. Petticrew, and A. Krysa, Improved Planar InAs Avalanche Photodiodes with Reduced Dark Current and Increased Responsivity. *J. Light. Technol.* 37, 1 (2019).
125. F. Wang, J. Chen, Z. Xu, Y. Zhou, and L. He, InAs-Based Type-II Superlattice Long Wavelength Photodetectors. *Quantum Sens. Nano Electron. Photonics XIII* 9755, 975519 (2016).
126. W. Huang, L. Lei, L. Li, J.A. Massengale, R.Q. Yang, T.D. Mishima, and M.B. Santos, Enhanced Collection Efficiencies and Performance of Interband Cascade Structures for Narrow Bandgap Semiconductor Thermophotovoltaic Devices. *J. Appl. Phys.* 124, 023101 (2018).
127. X.-C. Peng, Y. Liu, J.-J. Zou, and W.-J. Deng, *An Analysis on Device-Related Properties of the GaInSb Thermophotovoltaic Cell*. DEStech Trans. Environ. Energy Earth Sci. 336 (2018).
128. C.J. Hunter, F. Bastiman, A.R. Mohmad, R. Richards, J.S. Ng, S.J. Sweeney, and J.P.R. David, Absorption Characteristics of $GaAs_{1-x}Bi_x$/GaAs Diodes in the Near-Infrared. *IEEE Photonics Technol. Lett.* 24, 2191 (2012).
129. Y. Liu, X. Yi, N.J. Bailey, Z. Zhou, T.B.O. Rockett, L.W. Lim, C.H. Tan, R.D. Richards, and J.P.R. David, Valence Band Engineering of GaAsBi for Low Noise Avalanche Photodiodes. *Nat. Commun.* 12, 1 (2021).
130. J.M. Borrego, S. Saroop, R.J. Gutmann, G.W. Charache, T. Donovan, P.F. Baldasaro, and C.A. Wang, Photon Recycling and Recombination Processes in 0.53 EV p-Type InGaAsSb. *J. Appl. Phys.* 89, 3753 (2001).
131. S.R. Kurtz, A.A. Allerman, E.D. Jones, J.M. Gee, J.J. Banas, and B.E. Hammons, InGaAsN Solar Cells with 1.0 EV Band Gap, Lattice Matched to GaAs. *Appl. Phys. Lett.* 74, 729 (1999).
132. J. Borrego, M. Zierak, and G. Charache, Parameter extraction for TPV cell development, in *AIP Conference Proceedings*, vol. 371 (2008).
133. O.V. Sulima, GaSb-, InGaAsSb-, InGaSb-, InAsSbP-and Ge-TPV cells with diffused emitters, in *Photovoltaic Specialists Conference* (2002), pp. 892–895.
134. B. Bitnar, Silicon, Germanium and Silicon/Germanium Photocells for Thermophotovoltaics Applications. *Semicond. Sci. Technol.* 18, S221 (2003).
135. D. Let and G.V. Cimpoca, *Study Over Optical Absorption and Emission in Semiconductors*, J. Sci. Arts (2017).
136. M.A. Green, Solar Cells—Operating Principles, Technology and System Applications. *Sol. Energy* 28, 447 (1982).
137. P.J. Bishop and A.F. Gibson, Absorption Coefficient of Germanium at 10.6 μ. *Appl. Opt.* 12, 2549–2550 (1973).
138. H. Liu, S. Li, P. Sun, X. Yang, D. Liu, Y. Ji, F. Zhang, D. Chen, and Y. Cui, Study on Characterization Method of Optical Constants of Germanium Thin Films from Absorption to Transparent Region. *Mater. Sci. Semicond. Process.* 83, 58 (2018).
139. M. Huang, S. Li, P. Cai, G. Hou, T.I. Su, W. Chen, C.Y. Hong, and D. Pan, Germanium on Silicon Avalanche Photodiode. *IEEE J. Sel. Top. Quantum Electron.* 24, 1–11 (2018).
140. X. Guo, Q. Liu, H. Zhou, X. Luan, C. Li, Z. Hu, A. Hu, and X. He, High-Responsivity Si Photodiodes at 1060 Nm in Standard CMOS Technology. *IEEE Electron Device Lett.* 39, 228 (2018).
141. M.M. Gamel, P.J. Ker, W.E. Rashid, H.J. Lee, M.A. Hannan, and M.Z. Jamaludin, Performance of Ge and $In_{0.53}Ga_{0.47}$ As Thermophotovoltaic Cells Under Different Spectral Irradiances. *IEEE Access* 9, 37091 (2021).
142. N.H. Protik and D.A. Broido, Coupled Transport of Phonons and Carriers in Semiconductors: A Case Study of n-Doped GaAs. *Phys. Rev. B* 101, 75202 (2020).
143. Z. Utlu, Thermophotovoltaic Applications in Waste Heat Recovery Systems: Example of GaSb Cell. *Int. J. Low-Carbon Technol.* 15, 277 (2019).
144. N. Vandamme, H.L. Chen, A. Gaucher, B. Behaghel, A. Lemaître, A. Cattoni, C. Dupuis, N. Bardou, J.F. Guillemoles, and S. Collin, Ultrathin GaAs Solar Cells with a Silver Back Mirror. *IEEE J. Photovoltaics* 5, 565 (2015).
145. T. Manyk, K. Murawski, K. Michalczewski, K. Grodecki, J. Rutkowski, and P. Martyniuk, Method of Electron Affinity Evaluation for the Type-2 InAs/$InAs_{1-x}Sb_x$ Superlattice. *J. Mater. Sci.* 55, 5135 (2020).
146. Y. Liang, F. Wang, X. Luo, Q. Li, T. Lin, I.T. Ferguson, Q. Yang, L. Wan, and Z.C. Feng, Investigation of the Optical Properties of InSb Thin Films Grown on GaAs by Temperature-Dependent Spectroscopic Ellipsometry. *J. Appl. Spectrosc.* 86, 276 (2019).
147. C.Y. Tsai, Absorption Coefficients of Silicon: A Theoretical Treatment. *J. Appl. Phys.* 123, 183103 (2018).

148. M.C. Gupta and J. Ballato, *III–V Semiconductor Materials in The Handbook of Photonics*, 2nd ed., (Boca Raton: CRC Press, 2006).
149. M.W. Dashiell, J.F. Beausang, H. Ehsani, G.J. Nichols, D.M. Depoy, L.R. Danielson, P. Talamo, K.D. Rahner, E.J. Brown, S.R. Burger, P.M. Fourspring, W.F. Topper, P.F. Baldasaro, C.A. Wang, R.K. Huang, M.K. Connors, G.W. Turner, Z.A. Shellenbarger, G. Taylor et al., Quaternary InGaAsSb Thermophotovoltaic Diodes. *IEEE Trans. Electron Devices* 53, 2879 (2006).
150. T.S. Moss, Optical Absorption Edge in GaAs and Its Dependence on Electric Field. *J. Appl. Phys.* 32, 2136 (1961).
151. F. Stern and R.M. Talley, Optical Absorption in P-Type Indium Arsenide. *Phys. Rev.* 108, 158 (1957).
152. Y.-H. Lin and J.-F. Kiang, Efficiency Improvement of P-I-N Solar Cell By Embedding Quantum Dots. *Prog. Electromagn. Res.* 146, 167 (2014).
153. K.L. Lin, K.R. Catchpole, P. Campbell, and M.A. Green, High External Quantum Efficiency from Double Heterostructure InGaP/GaAs Layers as Selective Emitters for Thermophotonic Systems. *Semicond. Sci. Technol.* 19, 1268 (2004).
154. R. Ferrini, M. Patrini, and S. Franchi, Optical Functions from 0.02 to 6 EV of $Al_xGa_{1-X}Sb$/GaSb Epitaxial Layers. *J. Appl. Phys.* 84, 4517 (1998).
155. Z. Qiao, Y. Sun, W. He, Q. He, and C. Li, Polycrystalline GaSb Thin Films Grown by Co-Evaporation. *J. Semicond.* 30, 033004 (2009).
156. J.O. Akinlami, Optical Propertis of Gallium Antimonide GaSb. *Res. J. Phys.* 8, 17 (2014).
157. Y. Wang, N.F. Chen, X.W. Zhang, T.M. Huang, Z.G. Yin, Y.S. Wang, and H. Zhang, Evaluation of Thermal Radiation Dependent Performance of GaSb Thermophotovoltaic Cell Based on an Analytical Absorption Coefficient Model. *Sol. Energy Mater. Sol. Cells* 94, 1704 (2010).
158. A.K. Al-Mousoi, M.K.A. Mohammed, and H.A. Khalaf, Preparing and Characterization of Indium Arsenide (InAs) Thin Films by Chemical Spray Pyrolysis (CSP) Technique. *Optik (Stuttg)* 127, 5834 (2016).
159. G. Shen, Y. Zhao, Z. Dong, J. Liu, H. Xie, Y. Bai, and X. Chen, Enhancement of below Gap Transmission of InAs Single Crystal via Suppression of Native Defects. *Mater. Res. Express* 4, 036203 (2017).
160. R. Oetjen and H. Yoshinaga, Optical Properties of Indium Antimonide in the Region from 20 to 200 Microns. *Phys. Rev.* 101, 526 (1956).
161. E.J. Johnson, Absorption near the Fundamental Edge. *Semicond. Semimetals* 3, 153 (1967).
162. R. Vaillon, J.-P. Pérez, C. Lucchesi, D. Cakiroglu, P.-O. Chapuis, T. Taliercio, and E. Tournié, Micron-Sized Liquid Nitrogen-Cooled Indium Antimonide Photovoltaic Cell for near-Field Thermophotovoltaics. *Opt. Express* 27, A11 (2019).
163. Q. Lin, D. Sarkar, Y. Lin, M. Yeung, L. Blankemeier, J. Hazra, W. Wang, S. Niu, J. Ravichandran, Z. Fan, and R. Kapadia, Scalable Indium Phosphide Thin-Film Nanophotonics Platform for Photovoltaic and Photoelectrochemical Devices. *ACS Nano* 11, 5113 (2017).
164. G. García, P. Sánchez-Palencia, P. Palacios, and P. Wahnón, Transition Metal-Hyperdoped InP Semiconductors as Efficient Solar Absorber Materials. *Nanomaterials* 10, 5 (2020).
165. N. Manjula, A.R. Balu, K. Usharani, N. Raja, and V.S. Nagarethinam, Enhancement in Some Physical Properties of Spray Deposited CdO: Mn Thin Films through Zn Doping towards Optoelectronic Applications. *Optik (Stuttg)* 127, 6400 (2016).
166. M. Grundmann, Optical properties, in *The Physics of Semiconductors* (Springer, Berlin, 2010).
167. H. Sai, H. Mizuno, K. Makita, and K. Matsubara, Light Absorption Enhancement in Thin-Film GaAs Solar Cells with Flattened Light Scattering Substrates. *J. Appl. Phys.* 122, 123103 (2017).
168. L. Wang, Y. Yang, H. Ye, H. Alshehri, and Q. Ni, Plasmonic Light Trapping for Enhanced Light Absorption in Film-Coupled Ultrathin Metamaterial Thermophotovoltaic Cells. *Front. Energy* 12, 185 (2017).
169. Y. Wan, C.Y. Jiang, X.M. Wang, H.N. Liu, H. Wang, Z. Cai, and X. Guo, Ultrathin and Easy-Processing Photonic Crystal Absorbing Layers to Enhance Light Absorption Efficiency of Solar Cells. *APL Mater.* 7, 041113 (2019).
170. M. Tanenbaum and H.B. Briggs, Optical Properties of Indium Antimonide. *Phys. Rev.* 91, 1561 (2014).
171. S. Cao, Y. Zhao, S. Feng, Y. Zuo, L. Zhang, B. Cheng, and C. Li, Theoretical Analysis of InGaAs/InAlAs Single-Photon Avalanche Photodiodes. *Nanoscale Res. Lett.* 14, 1–8 (2019).
172. O.V. Sulima, GaSb-, InGaAsSb-, InGaSb-, InAsSbP- and Ge-TPV Cells for Low-Temperature TPV Applications, in *AIP Conference Proceedings*, vol. 653 (AIP, 2003), pp. 434–441.
173. S. Xie, C. Yang, S.S. Huang, Y. Yuan, Y. Zhang, J. Shang, C. Cai, Y. Zhang, Y. Xu, H. Ni, and Z. Niu, 2.1 μm InGaSb Quantum Well Lasers Exhibiting the Maximum Conversion Efficiency of 2.75% with Digitally Grown AlGaAsSb Barriers and Gradient Layers. *Superlattices Microstruct.* 130, 339 (2019).
174. D. Li, C. Lan, A. Manikandan, S.P. Yip, Z. Zhou, X. Liang, L. Shu, Y.L. Chueh, N. Han, and J.C. Ho, Ultra-Fast Photodetectors Based on High-Mobility Indium Gallium Antimonide Nanowires. *Nat. Commun.* 10, 1 (2019).
175. A. Rogalski, P. Martyniuk, M. Kopytko, P. Madejczyk, and S. Krishna, Inassb-Based Infrared Photodetectors: Thirty Years Later On. *Sensors (Switzerland)* 20, 7047 (2020).
176. M. Hinojosa, I. García, I. Rey-Stolle, and C. Algora, Inverted Rear-Heterojunction GaInP Solar Cells Using Te Memory Effect. *Sol. Energy Mater. Sol. Cells* 205, 110235 (2020).
177. M.S. Alam, M.S. Rahman, M.R. Islam, A.G. Bhuiyan, and M. Yamada, Refractive index, absorption coefficient, and photoelastic constant: key parameters of InGaAs material relevant to InGaAs-based device performance, in *International Conference on Indium Phosphide & Related Materials* (2007), p. 343.
178. P.T. Webster, N.A. Riordan, S. Liu, E.H. Steenbergen, R.A. Synowicki, Y.H. Zhang, and S.R. Johnson, Measurement of InAsSb Bandgap Energy and InAs/InAsSb Band Edge Positions Using Spectroscopic Ellipsometry and Photoluminescence Spectroscopy. *J. Appl. Phys.* 118, 245706 (2015).
179. H. Baaziz, Z. Charifi, A.H. Reshak, B. Hamad, and Y. Al-Douri, Structural and Electronic Properties of GaN_xAs_{1-x} Alloys. *Appl. Phys. A Mater. Sci. Process.* 106, 687 (2012).
180. U. Tisch, E. Finkman, and J. Salzman, The Anomalous Bandgap Bowing in GaAsN. *Appl. Phys. Lett.* 81, 463 (2002).
181. M. Gamel, P.J. Ker, H.J. Lee, W.E.S.W.A. Rashid, M.A. Hannan, J. David, and M.Z. Jamaludin, Multi-Dimensional Optimization of $In_{0.53}Ga_{0.47}$ As Thermophotovoltaic Cell Using Real Coded Genetic Algorithm. *Nat. Sci. Rep.* 11, 1–4 (2021).
182. X. Peng, B. Zhang, G. Li, J. Zou, Z. Zhu, Z. Cai, S. Zhou, Y. Li, Z. Wang, and W. Jiang, Simulation of Temperature-Dependent Material Parameters and Device Performances for GaInAsSb Thermophotovoltaic Cell. *Infrared Phys. Technol.* 54, 454 (2011).
183. Z.A. Shellenbarger, High performance InGaAsSb TPV cells, in *AIP Conference Proceedings*, vol. 738 (AIP, 2004), pp. 345–352.
184. X. Peng, X. Guo, B. Zhang, X. Li, X. Zhao, X. Dong, W. Zheng, and G. Du, Numerical Analysis of the Short-Circuit Current Density in GaInAsSb Thermophotovoltaic Diodes. *Infrared Phys. Technol.* 52, 152 (2009).
185. M. Mitsuhara, Y. Ohiso, and H. Matsuzaki, Strain-Compensated InGaAsSb/InGaAsSb Multiquantum-Well Structure Grown

on InP (0 0 1) Substrate as Optical Absorber for Wavelengths beyond 2 Mm. *J. Cryst. Growth* 535, 125551 (2020).
186. S. Kurtz, J.F. Geisz, D.J. Friedman, J.M. Olson, A. Duda, N.H. Karam, R.R. King, J.H. Ermer, and D.E. Joslin, Modeling of electron diffusion length in GaInAsN solar cells, in *Conference Record of the IEEE Photovoltaic Specialists Conference*, vol. 2000-Janua (IEEE, 2000), pp. 1210–1213.
187. J.F. Geisz, D.J. Friedman, J.M. Olson, S.R. Kurtz, and B.M. Keyes, Photocurrent of 1 EV GaInNAs Lattice-Matched to GaAs. *J. Cryst. Growth* 195, 401 (1998).
188. M. Seifikar, E.P. O'Reilly, and S. Fahy, Optical Absorption of Dilute Nitride Alloys Using Self-Consistent Green's Function Method. *Nanoscale Res. Lett.* 9, 1 (2014).
189. S.J. Sweeney, K. Hild, and S. Jin, The potential of GaAsBiN for multi-junction solar cells, in *Conference Record of IEEE Photovoltaic Specialists Conference (PVSC)* (2013), p. 2474.
190. W.Q. Jemmali, N. Ajnef, M.M. Habchi, and A. Rebey, Theoretical Study of Strained GaNAsBi/GaAs Quantum Structures for Application in Infrared Range. *Mater. Sci. Semicond. Process.* 125, 105615 (2021).
191. N. Ajnef, W.Q. Jemmali, M.M. Habchi, and A. Rebey, Biaxial Strain Effects on the Band Structure and Absorption Coefficient of $GaAs_{1-x-Y}N_xBi_y$/GaAs MQWs Calculated Using k.p Method. *Optik Stuttg.* 223, 165484 (2020).
192. S. Wang, T. Jin, S. Zhao, D. Liang, and P. Lu, Phosphorus and nitrogen containing dilute bismides, in vol. 285 (Springer Singapore, 2019), pp. 97–123.
193. M. Su, C. Li, P. Yuan, F. Rao, Y. Jia, and F. Wang, Electronic and Optical Properties of Quaternary Alloy GaAsBiN Lattice-Matched to GaAs. *Opt. Express* 22, 30633 (2014).
194. S. Lee, S. H. Kodati, B. Guo, A. H. Jones, M. Schwartz, H. Jung, N. Pfiester, M. Winslow, C. H. Grein, T. J. Ronningen, J. C. Campbell, and S. Krishna, Thick $Al_{0.85}Ga_{0.15}As_{0.56}Sb_{0.44}$ avalanche photodiodes on InP substrate, in *Infrared Technology and Applications XLVII*, edited by G.F. Fulop, M. Kimata, L. Zheng, B.F. Andresen, and J.L. Miller (SPIE, 2021), p. 4.
195. A. Abdulkadir, A.A. Aziz, and M.Z. Pakhuruddin, Impact of Micro-Texturization on Hybrid Micro/Nano-Textured Surface for Enhanced Broadband Light Absorption in Crystalline Silicon for Application in Photovoltaics. *Mater. Sci. Semicond. Process.* 105, 104728 (2020).
196. K. Mertens, Fundamentals of semiconductor physics, in *Photovoltaics: Fundamentals, Technology and Practice* (Wiley, Chichester, 2014).
197. M. Mohammed, A. Gamel, H.J. Lee, W. Emilin, S. Wan, A. Rashid, P.J. Ker, L.K. Yau, M.A. Hannan, and Z. Jamaludin, A Review on Thermophotovoltaic Cell and Its Applications in Energy Conversion: Issues and Recommendations. *Materials (Basel)* 14, 4944 (2021).